REPORT OF POSDOCTORAL RESEARCH.

EXTENDED STEINMETZ EQUATION.

H. E. TACCA y C. R. SULLIVAN.

EXTENDED STEINMETZ EQUATION

REPORT OF POSDOCTORAL RESEARCH

presented by

Hernán Emilio Tacca

(Postdoctoral visitor researcher from 2/02 to 10/02)

Research Director: Prof. Charles R. Sullivan

THAYER SCHOOL OF ENGINEERING, October 2002.

To María Cecilia Foncuberta

EXTENDED STEINMETZ EQUATION (ESE)

***Abstract.* -** A modified Steinmetz equation suitable for non-sinusoidal operation of magnetic components is presented. The proposed expression has coefficients that may be obtained from the original Steinmetz equation using analytical formulas. Moreover, the functions involved are widely used in daily work in electrical engineering. This leads to simple and general electrical formulas suitable for magnetic power loss estimation in symmetrical power converter design. Using a fitting approach, the model is later extended to cover asymmetrical converter magnetic component applications.

***Keywords.* -** Magnetic core losses, Steinmetz equation, power magnetic components, switching converters.

ECUACIÓN DE STEINMETZ EXTENDIDA (ESE)

***Resumen.* -** Se propone una modificación de la ecuación de Steinmetz para extender su aplicación a regímenes de operación no senoidales. La expresión propuesta incorpora coeficientes que pueden ser determinados a partir de la ecuación original de Steinmetz por medio de expresiones analíticas. Además, las funciones matemáticas involucradas son de uso habitual en ingeniería eléctrica. Esto permite obtener fórmulas generales, pero simples, aplicables al proyecto de convertidores de estructura simétrica.
Utilizando un procedimiento de ajuste empírico, el modelo es luego ampliado para servir en proyectos de componentes para convertidores asimétricos.

***Palabras clave.* -** Pérdidas magnéticas, ecuación de Steinmetz, componentes magnéticos de potencia, convertidores conmutados.

ACKNOWLEDGEMENTS

This work was done thanks a sabbatical staying at Thayer School of Engineering granted by the University of Buenos Aires (Argentina) and the Dartmouth College (U.S.A.).

I wish to thank the continuing support of Prof. Charles R. Sullivan, who constantly encouraged me with infinite patience and guidance, allowing this work to be possible. I will be ever grateful.

I am also indebted to Kathleen Tippit for kindly helping me with the daily work.

I would like to thank Carlos A. Godfrid and José P. Cebreiro for the valuable services provided at Buenos Aires, during my postdoctoral staying in Thayer School.

The United States Department of Energy (D.O.E.), making research like this possible, provided the funding for this work.

INDEX

PART I

EXTENDED STEINMETZ EQUATION PRINCIPLES AND FORMULATION

I - 1. INTRODUCTION

Magnetic losses may be considered due to the hysteresis phenomenon and eddy current circulation inside the core.

For sinusoidal waveforms, the hysteresis losses may be obtained from an empirical expression due to the work of C. P. Steinmetz:

$$p_{v_H} = \frac{P_H}{Vol} = k_h \; f \; B_m{}^{\varsigma} \tag{1.1.a}$$

where k_h and ς are constant to be experimentally determined, while B_m is the maximum of the induction.

On the other hand, the eddy current losses are given by:

$$p_{v_E} = \frac{P_E}{Vol} = k_e \; \frac{1}{\rho} \; f^2 \; B_m{}^2 \tag{1.1.b}$$

where ρ is the core material resistivity.

In order to take account of the anomalous eddy current losses due to a non-homogeneous current distribution (eddy currents), the resistivity may be assumed to be frequency dependent.

Thus, an approximative formula giving the total losses results:

$$p_v = \frac{P}{Vol} = k_h \; f \; B_m{}^{\varsigma} + k_e \; \frac{1}{\rho(f)} \; f^2 \; B_m{}^2 \tag{1.1.c}$$

To simplify the parameter extraction from experimental data, the above equation may be reduced to:

$$p_v = \frac{P}{Vol} = k_s \; f^{\alpha} \; B_m{}^{\beta} \tag{1.2}$$

where k_s , α , and β are constants to be determined from experimental data.

This last expression is usually known as Steinmetz equation.

Unfortunately, in power electronics most of the waveforms are not sinusoidal and eq. 1.2 is no longer valid.

For non-sinusoidal waveforms the eddy current losses may be expressed as [1]:

$$p_{vE} = k_E \; \frac{1}{\rho(f)} \left(\dot{B}_{rms} \right)^2 \tag{1.3.a}$$

while, for symmetrical waveforms without minor loops, the hysteresis losses remain expressed as function of the induction amplitude $\Delta B = 2 \; B_m$, as:

$$p_{v_H} = k_H \; f \left(\frac{\Delta B}{2} \right)^{\varsigma} \tag{1.3.b}$$

Therefore, the total losses can be expressed as:

$$p_v = k_H \; f \left(\frac{\Delta B}{2} \right)^{\varsigma} + k_E \; \frac{1}{\rho(f)} \left(\dot{B}_{rms} \right)^2 \tag{1.3.c}$$

A simplification similar to what was done with eq. 1.c may be introduced in order to transform the eq. 1.3.c into a single product:

$$p_v = k_G \; f^{\nu} \left(\frac{\Delta B}{2} \right)^{\chi} \left(\dot{B}_{rms} \right)^{\zeta} \tag{1.4}$$

This equation is consistent with the classical Steinmetz expression, provided that appropriate values are assigned to the constants k_G , ν , χ ,and ζ to force eq. 1.4 becoming equal to eq. 1.2 for sinusoidal waveforms .

However, expression 1.4 has still an important drawback for cases other than pure sinusoids: A single frequency has to be adopted to do calculations.

To overcome this limitation, an equivalent frequency is defined as:

$$f_{eq} = \frac{1}{2}\,\frac{1}{\Delta B}\left(\frac{1}{T}\int_0^T \left|\frac{dB}{dt}\right| dt\right) = \frac{\left|\dot{B}\right|_{av}}{2\,\Delta B} \qquad (1.5)$$

(for pure sinewaves eq. 1.5 yields $f_{eq} = f$).

Substituting 1.5 into 1.4 yields:

$$p_v = \frac{P}{Vol} = k_m \left(\dot{B}_{rms}\right)^{\gamma} \left(\left|\dot{B}\right|_{av}\right)^{\varepsilon} \left(\frac{\Delta B}{2}\right)^{\xi} \qquad (1.6.a)$$

where,

$$\dot{B}_{rms} = \sqrt{\frac{1}{T}\int_0^T \left(\frac{dB}{dt}\right)^2 dt} \qquad (1.6.b)$$

$$\left|\dot{B}\right|_{av} = \frac{1}{T}\int_0^T \left|\frac{dB}{dt}\right| dt \qquad (1.6.c)$$

$$\Delta B = B_{\max} - B_{\min} \qquad (1.6.d)$$

for symmetrical waveforms it is $\Delta B = 2\,B_m$, where B_m is the amplitude of $B_{(t)}$.

Equation 1.6.a is a Steinmetz-like expression generalized for non-sinusoidal operation, dependent on dB/dt, but expressing it by means of analytical functions of *B*.

For sinusoidal waveforms eq. 1.6.a must match the classical Steinmetz equation 1.2.

Therefore:

$$k_s = k_m \left(\sqrt{2}\,\pi\right)^{\gamma} 4^{\varepsilon} \qquad (1.7.a)$$

$$\alpha = \gamma + \varepsilon \qquad (1.7.b)$$

$$\beta = \gamma + \xi + \varepsilon \qquad (1.7.c)$$

From eqs. 1.7 the following expression results:

$$p_v = \frac{P}{Vol} = \frac{k_s}{\left(\sqrt{2}\,\pi\right)^{\alpha}\left(\frac{\sqrt{8}}{\pi}\right)^{\varepsilon}} \left(\dot{B}_{rms}\right)^{\alpha-\varepsilon} \left(\left|\dot{B}\right|_{av}\right)^{\varepsilon} \left(\frac{\Delta B}{2}\right)^{\beta-\alpha} \qquad (1.8).$$

Eq. 1.8 will be named the *Extended Steinmetz Equation (ESE)* . It includes a parameter ε , which modifies the rise of the plotted function (loss vs. duty cycle). This parameter should be determined looking for the best fit with experimental data.

Another modified Steinmetz equation, the iGSE [2][3] proved to match the measured experimental values well, so the ESE will be compared against the iGSE when experimental values are not available.

In Fig. 1.1 , the ESE is compared with results obtained from the iGSE , for a triangular waveform with variable duty cycle D , using a ferrite core made of 3C85 material [2]. For this material, the best ε value is 0.9 , which gives the best agreement with the iGSE.

For others materials, the optimal ε varies.

It is found that the optimal ε does not depend on β nor k_s , but it is affected by α .

As α usually ranges from 1.1 to 1.7 , a linear function is proposed for ε :

$$\varepsilon = k_{\varepsilon 1} + k_{\varepsilon 2}\ \alpha \qquad (1.9).$$

For $1.1 \le \alpha \le 1.7$ a good match with the iGSE (and also with experimental data) is obtained adopting:

$$\varepsilon = 2 - 0.86\ \alpha \qquad (1.10).$$

Figures 1.2 to 1.4 show how the ESE matches the iGSE results for different sets of Steinmetz parameters (using the ε given by eq. 1.10).

In order to test the agreement with the iGSE , two sinusoidal waveforms with different frequencies are utilized [3]. So, the induction is,

$$B_{(t)} = B_m\left[c \sin \omega t + (1-c)\sin 3\omega t\right] \qquad (1.11).$$

The obtained results are plotted in Fig. 1.5 , as function of c , which is the amplitude proportion of each sinusoidal component.

Notice that a very good agreement with the GSE [2] is found when the minor loops effect is not considered. (This calls for some way of considering multiple minor loops using the ESE).

As a great variety of converters have no minor loops during normal operation, in the next section the ESE will be applied to symmetrical converters assuming no minor loops exist.

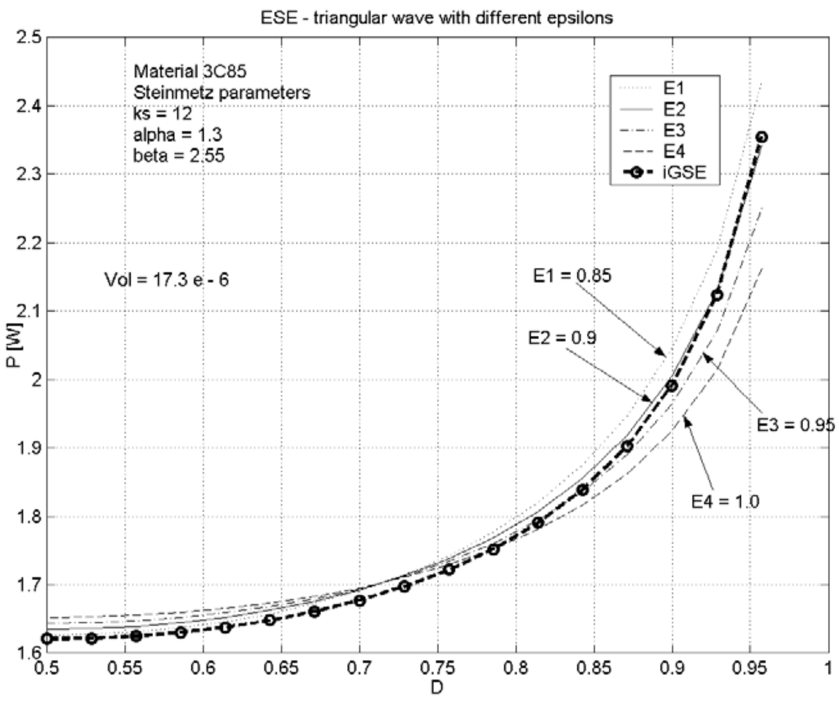

Fig. 1.1 : Plot of ESE with different ε values, compared vs. iGSE.

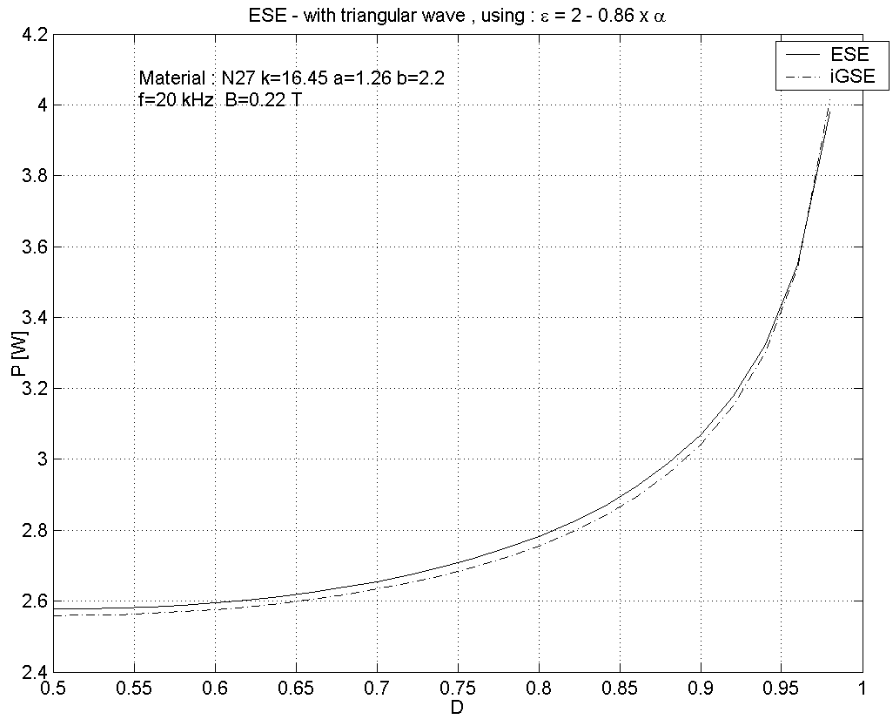

Fig. 1.2 : Plot of ESE and iGSE with triangular waveform for material N27.

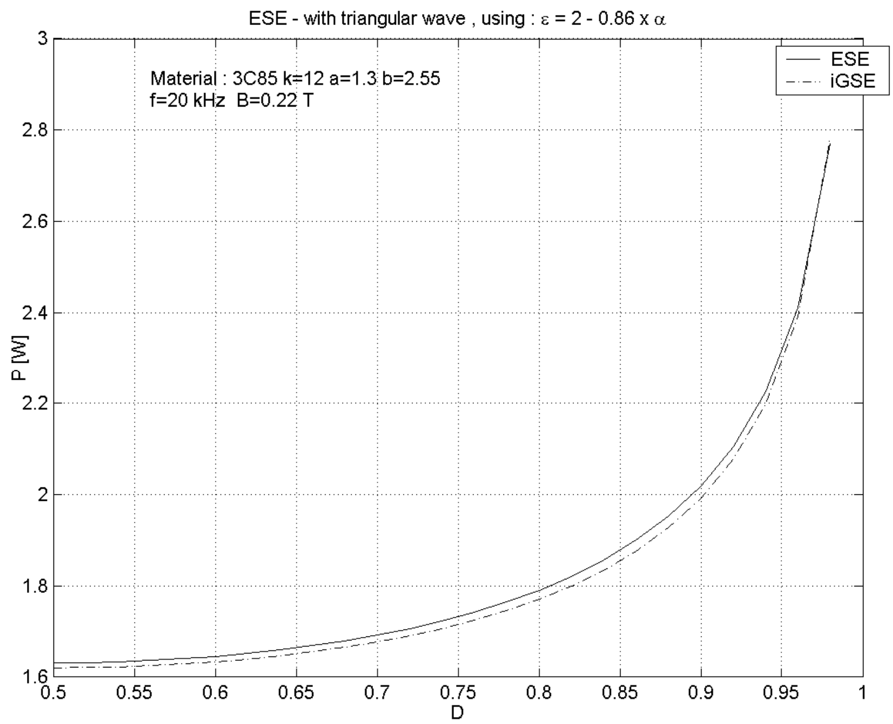

Fig. 1.3 : Plot of ESE and iGSE with triangular waveform for material 3C85.

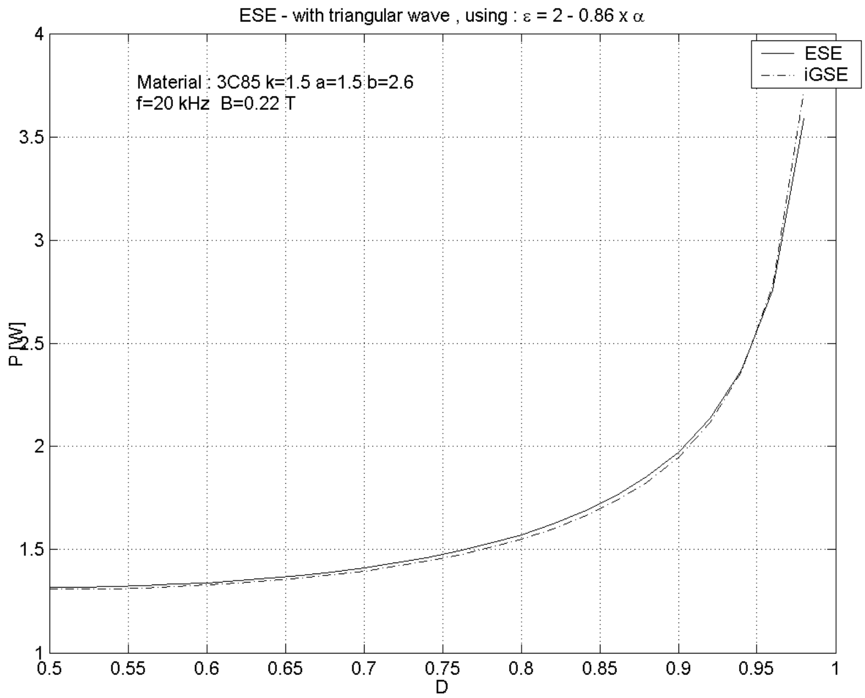

Fig. 1.4 : Plot of ESE and iGSE with triangular waveform for material 3C85 using the set of Steinmetz parameters for 200 kHz (even with 20 kHz).

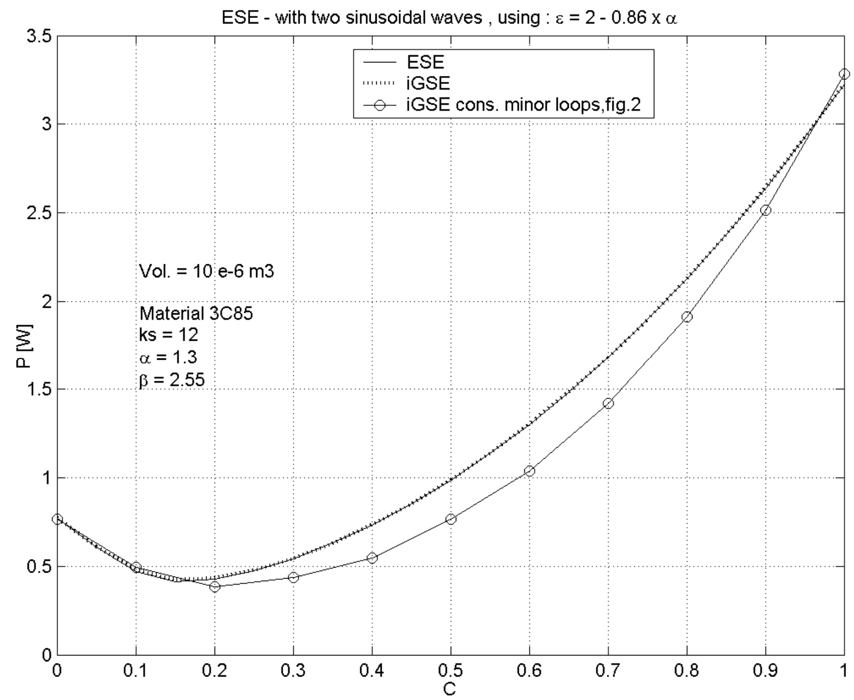

Fig. 1.5 : Plot of ESE and iGSE with two sinusoidal waveforms for material 3C85 .

I - 2. APPLICATION OF THE ESE TO SYMMETRICAL CONVERTERS

I - 2.1 *Principles*

Adopting the value of the parameter given by eq. 1.10 , the ESE may be expressed as:

$$p_v = \frac{P}{Vol} = \frac{1.234}{(4.863)^\alpha} k_s \left(\dot{B}_{rms}\right)^{(1.86\,\alpha-2)} \left(\left|\dot{B}\right|_{av}\right)^{(2-0.86\,\alpha)} \left(\frac{\Delta B}{2}\right)^{\beta-\alpha} \qquad (1.12).$$

Considering:

$$\frac{\left(\dot{B}_{rms}\right)}{\left(\left|\dot{B}\right|_{av}\right)} = \frac{V_{rms}}{|V|_{av}} = f_{fV} \qquad (1.13)$$

where f_{fV} is the shape factor of the applied voltage, the ESE may be rearranged yielding:

$$p_v = \frac{P}{Vol} = \frac{1.234}{(4.863)^\alpha} k_s \left(f_{fV}\right)^{(0.86\,\alpha-2)} \left(\dot{B}_{rms}\right)^{\alpha} \left(\frac{\Delta B}{2}\right)^{\beta-\alpha} \qquad (1.14)$$

where:

$$\dot{B}_{rms} = \frac{V_{rms}}{n\, S_{Fe}} \qquad (1.15)$$

Dividing eq. 1.14 by the Steinmetz equation (2) (assuming $\Delta B = 2\, B_m$) and substituting eq. 1.15 one obtains:

$$\frac{p_v}{p_{v\,Stm}} = \frac{1.234}{(4.863)^\alpha} \left(f_{fV}\right)^{(0.86\,\alpha-2)} \left(\frac{V_{rms}}{n\, S_{Fe}}\right)^{\alpha} \left(\frac{\Delta B}{2}\right)^{-\alpha} f^{-\alpha} \qquad (1.16)$$

For unipolar voltages waveforms (see examples in Fig. 1.6):

$$\Delta B = \frac{1}{n\, S_{Fe}} \int_0^{T/2} v_{(t)}\, dt = \frac{|V|_{av}}{2\, f\, n\, S_{Fe}} \qquad (1.17)$$

then, substituting eq. 1.17 into eq. 1.16 and using definition 13 yields:

$$\frac{p_v}{p_{v\,Stm}} = 1.234\, \left(0.82254\right)^{\alpha} \left(f_{fV}\right)^{(1.86\,\alpha\,-\,2)} \qquad (1.18).$$

Notice that to obtain p_v no assumptions were made neither on the type of converter nor in its waveforms, except for the unipolar waveform feature required.

For a typical $\alpha = 1.3$ a square wave converter yields $p_v / p_{v\,Stm} = 0.957$.

A rectangular wave inverter having a sinusoidal equivalent wave shape factor of $f_{fV} = 1.11$ (duty = 0.812) gives $p_v \big/ p_{v\,Stm} = 0.9996 \cong 1$. For a duty-cycle of 0.25 one obtains $p_v \big/ p_{v\,Stm} = 1.28$, but this is a quite small duty for typical nominal power operation.

Next, an example of application to a complex output waveform converter is presented.

I - 2.2 ***Example:***

Unipolar PWM Sine Wave Inverter

For an inverter using unipolar PWM sine wave synthesis (as shown in Fig. 1.7), the average transformer voltage must be:

$$V_P \; d_{(t)} = V_m \; \sin\omega\, t \qquad \text{(E1.1)}$$

where $d_{(t)}$ is the duty cycle required to produce the sinusoidal average value of the output signal. So,

$$d_{(t)} = \frac{V_m}{V_P} \sin\omega\, t \qquad \text{(E1.2).}$$

If $V_m = V_P$ the rms voltage applied to the transformer becomes:

$$V_{rms} = \sqrt{\frac{2}{T}\int_0^{T/2} V_P{}^2 \; d_{(t)} \; dt} = V_P \sqrt{\frac{2}{T}\int_0^{T/2} \sin\omega\, t \; dt} = \sqrt{\frac{2}{\pi}}\, V_P \qquad \text{(E1.3)}$$

and the average rectified value results:

$$|V|_{av} = \frac{2}{T}\int_0^{T/2} V_P \; d_{(t)} \; dt = \frac{2}{\pi} V_P \qquad \text{(E1.4).}$$

Therefore, the voltage shape factor is: $f_{fV} = \sqrt{\frac{\pi}{2}} = 1.2533$. From eq. 18, for $\alpha = 1.3$ this yields:

$$p_v \big/ p_{v\,Stm} = 1.10 \qquad \text{(E1.5)}$$

A 10% of increase over the magnetic losses obtained from the classical Steinmetz equation should be expected in a transformer used for this application.

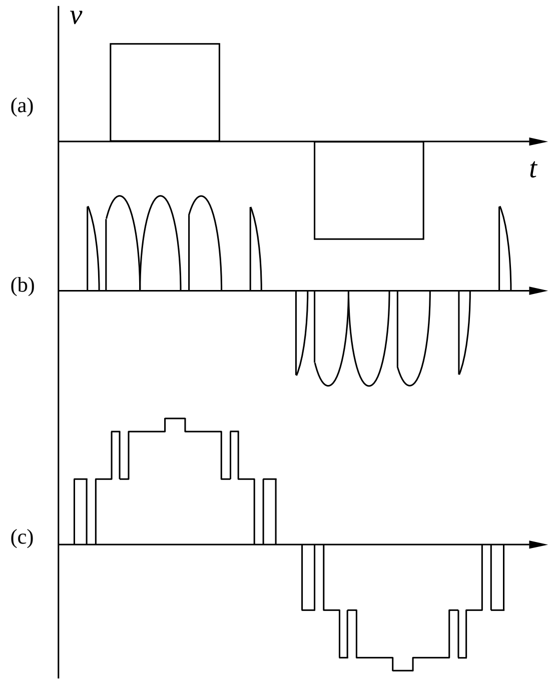

Fig. 1.6 : Examples of unipolar waveforms, (a) rectangular wave inverter, (b) cycloconverter, (c) multilevel inverter.

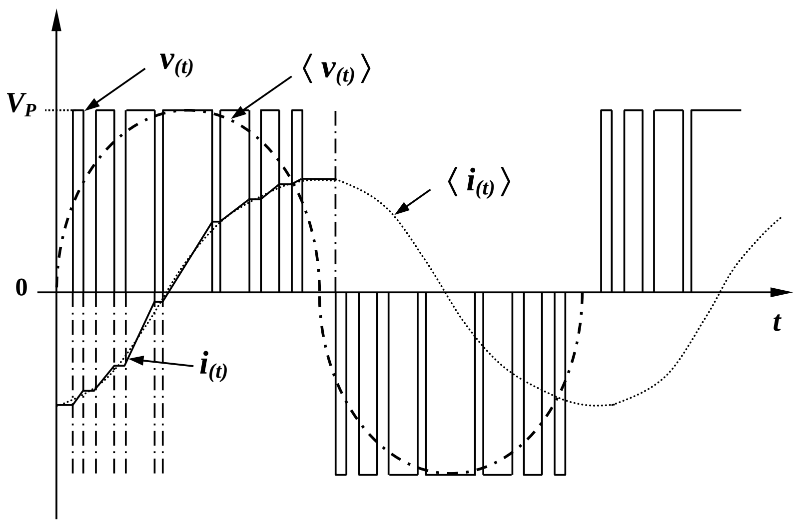

Fig. 1.7 : Unipolar PWM waveforms (local average values in dashed lines).

I - 3. CORRECTION FOR MULTIPLE LOOP CONSIDERATION

I - 3.1 *Principles*

If only the maximum loop amplitude $\Delta B_m = B_{\max} - B_{\min}$ is considered, when multiple loops appear, the ESE gives results higher than the experimental ones.

To overcome this problem, the flux waveform is separated in individual loops without including inner loops, following the procedure introduced in [3]. Thus, the calculated losses for each separate loop are added weighting its contributions using the proportion of time spent by each separate loop.

An algorithm implemented as MATLAB function is presented. It works with sampled data entered as a vector file.

The shape of the minor loops depends on the sequence in which they are separated, but the total losses must be the same regardless the algorithm used.

In order to show that the total loss calculation does not depend on the method of minor loop separation two alternatives are presented: In case of multiple maximum, the first algorithm takes the first maximum found as boundary for the rising part of the whole loop, while the remaining section of the loop is considered as the falling part. The other alternative takes the last maximum encountered as rising part limit and the remaining is assumed to be the fall part.

Results show that even if the minor loop computed losses are different, the total losses obtained are the same.

In order to test the proposed model, its predictions are compared against the iGSE and experimental data. As in the former case (without minor loop correction) the agreement with the iGSE results are quite good (both curves practically coincide).

Fig. 1.8 presents the flow chart of the basic function used for minor loop separation. The MATLAB code is included as appendix.

I - 3.2 *Test against iGSE and experimental data*

For two merged variable amplitude sinusoidal waveforms, the Fig. 1.9 shows the plot of ESE corrected for minor loops vs. ESE without correction and GSE (that is iGSE without considering minor loops), and also the experimental data and the iGSE (GSE corrected for minor loops). The ESE and GSE without correction practically coincide, as do the experimental values with iGSE and the corrected ESE. Meanwhile, a remarkable disparity between experimental values and uncorrected ESE (and GSE) arises when multiple loops appear as c increases.

Fig. 1.10 shows the results obtained when using both algorithm alternatives above mentioned. Notice the curves practically coincide.

On the other hand, Fig. 1.11 presents the comparison between ESE (correcting for minor loops), ESE without minor loops correction and experimental values, when applying fixed-amplitude merged sine waves, while phase between the component waves is varied.

I - 3.3 *Bipolar PWM Sine Wave Inverter*

In bipolar PWM there are multiple voltage commutations, each one corresponding to an inflexion point of the magnetizing current I_{M_i} (see Fig. 1.12) and so also to an inflection point of the induction B_i .

In Fig. 1.13 a switching cycle is detailed. There, the major loop passes through points 2, 3, 5, and 6, while points 3, 4, and 5 form a minor loop.

The major loop might be produced by a voltage waveform having a voltage $+V_P$ during $\Delta t_{P_{eq}}$ and 0 V during $\Delta t_{Z_{eq}}$.

Therefore, for this equivalent voltage waveform the shape factor will be the same obtained for unipolar

PWM (that is, $f_{fV} = \sqrt{\frac{\pi}{2}} = 1.2533$), so the major loop will have losses increased with respect the case of sinusoidal driving by a factor: $p_v / p_{v\ Stm} = 1.10$, as stated by eq. E1.5 .

To compute the total losses, the minor loop losses have to be calculated in order to be added to the major loop ones.

From Fig. 1.13 one obtains:

$$\left|\frac{dB}{dt}\right| = \frac{\Delta B_j}{\Delta t_{n_j}} = \frac{V_P}{n_P\ S_{Fe}} \tag{1.19}$$

$$\Delta t_{Z_{eq}} = 2\ \Delta t_{n_j} \tag{1.20}$$

As the derivative of the induction is a square wave, it follows that:

$$\dot{B}_{rms} = \left|\dot{B}\right|_{av} = \left|\frac{dB}{dt}\right| = \frac{\Delta B_j}{\Delta t_{n_j}} = \frac{V_P}{n_P\ S_{Fe}} \tag{1.21}$$

Substituting these values into the ESE expression (eq. 1.12) and weighting the minor loop loss contribution by its time duration yields:

$$p_{V_{ML}\ j} = k_m \left(\frac{\Delta B_j}{\Delta t_{n_j}}\right)^{\alpha} \left(\frac{\Delta B_j}{2}\right)^{\beta-\alpha} \frac{2\ \Delta t_{n_j}}{T} \tag{1.22}$$

where,

$$k_m = \frac{1.234}{(4.863)^{\alpha}}\ k_s \tag{1.23}$$

and $T = 1/f$ is the period of sinewave to be synthesized.

Substituting eq. 1.21 into eq. 1.22 gives:

$$p_{V_{ML}\ j} = 2^{\alpha-\beta+1}\ k_m\ f \left(\frac{V_P}{n_P\ S_{Fe}}\right)^{\beta} \Delta t_{n_j}{}^{\beta-\alpha+1} \tag{1.24}$$

From Fig. 1.13, it may be seen that in order to synthesize a sinewave we must have:

$$V_P\left(T_{SW} - \Delta t_{n_j}\right) - V_P\ \Delta t_{n_j} = \left(V_P\ \sin\omega\, t_j\right) T_{SW} \tag{1.25}$$

From eq. 1.25 :

$$\Delta t_{n_j} = \frac{T_{SW}}{2}\left(1 - \sin\omega\, t_j\right) \tag{1.26}$$

Substituting eq. 1.26 into eq. 1.24 gives:

$$p_{V_{ML}\ j} = 2^{2(\alpha-\beta)}\ k_m\ \frac{f}{f_{SW}{}^{\beta-\alpha+1}} \left(\frac{V_P}{n_P\ S_{Fe}}\right)^{\beta} \left(1 - \sin\omega\, t_j\right)^{\beta-\alpha+1} \tag{1.27}$$

This expression is valid for the minor loops belonging to the rise part of induction wave; thus it will be valid for computing the minor loops losses during half of the induction wave cycle.

Due to the symmetry of the induction waveform, the total minor loop losses will be twice the value of the rising part ones. Therefore:

$$p_{V_{ML}} = 2\sum_{j=1}^{n/2} p_{V_{ML}\ j} = n\left(\frac{2}{n}\sum_{j=1}^{n/2} p_{V_{ML}\ j}\right) = n\left\langle p_{V_{ML}\ j}\right\rangle \tag{1.28}$$

where n is the number of minor loops per cycle of the synthesized sinewave:

$$n = f_{SW} / f \tag{1.29}$$

As $f_{SW} >> f$ the discrete average may be approximated by the integral average and using eq. 1.29 it results:

$$p_{V_{ML}} = 2^{2(\alpha-\beta)}\ k_m\ f_{SW}{}^{\alpha-\beta} \left(\frac{V_P}{n_P\ S_{Fe}}\right)^{\beta} \left(\frac{2}{\pi}\int_0^{\pi/2}(1-\sin\theta)^{\beta-\alpha+1}d\theta\right) \qquad (1.30).$$

The integral between brackets should be calculated numerically but for $1.5 \le \beta-\alpha+1 \le 3$ it may be approximated with less than 0.6 % of error by:

$$S = \left(\frac{2}{\pi}\int_0^{\pi/2}(1-\sin\theta)^{\beta-\alpha+1}d\theta\right) \cong \frac{0.38}{(\beta-\alpha+1)^{0.75}} \qquad (1.31).$$

Usually $\beta-\alpha+1 \cong 2$ and the integral approaches the value 0.23.

Substituting eqs. 1.23 and 1.31 into eq. 1.30 yields:

$$p_{V_{ML}} = 1.234\,(0.25)^{\beta}\ (0.8225)^{\alpha}\ k_s\ f_{SW}{}^{\alpha-\beta} \left(\frac{V_P}{n_P\ S_{Fe}}\right)^{\beta} S \qquad (1.32).$$

Dividing eq. 1.32 by the Steinmetz's equation:

$$\frac{p_{V_{ML}}}{p_{V_{Stm}}} = 1.234\ \frac{(0.25)^{\beta}\ (0.8225)^{\alpha}}{f\ f_{SW}{}^{\beta-\alpha}} \left(\frac{V_P}{n_P\ S_{Fe}\ B_m}\right)^{\beta} S \qquad (1.33)$$

where,

$$B_m = B_{S_m} + \frac{\left|\Delta B\ _{T_{SW}/2}\right|}{2} \qquad (1.34)$$

is the maximum induction value, B_{S_m} is the peak value of the sinusoidal local average induction, and $\left|\Delta B\ _{T_{SW}/2}\right|$ is the amplitude of the alternative high frequency component of the induction, when it reaches it maximum value. This happens each time the primary local average voltage crosses through zero. Therefore, the duty cycle must be 1/2, which yields:

$$\left|\Delta B\ _{T_{SW}/2}\right| = \frac{V_P}{2\ f_{SW}\ n_P\ S_{Fe}} \qquad (1.35).$$

Assuming a primary peak voltage for the synthesized sinewave equal to V_P , from Faraday's law one obtains:

$$V_P = 2\,\pi\ f\ n_P\ S_{Fe}\ B_{S_m} \qquad (1.36).$$

Substituting eqs. 1.34, 1.35 and 1.36 into eq. 1.33 yields:

$$\frac{p_{V_{ML}}}{p_{V_{Stm}}} = 1.234\,\frac{(0.25)^{\beta}\ (0.8225)^{\alpha}}{f\ f_{SW}{}^{\beta-\alpha}} \left(\frac{4\ f_{SW}}{1+\dfrac{2}{\pi}\ \dfrac{f_{SW}}{f}}\right)^{\beta} S \qquad (1.37).$$

Assuming $f_{SW} >> f$ the eq. 1.37 becomes:

$$\frac{p_{V_{ML}}}{p_{V_{Stm}}} = 1.234\,\frac{(0.25)^{\beta}\ (0.8225)^{\alpha}}{f\ f_{SW}{}^{\beta-\alpha}}\,(2\,\pi\ f)^{\beta}\ S$$

which may be rearranged as:

$$\frac{p_{V_{ML}}}{p_{V_{Stm}}} = 1.234\,(0.8225)^{\alpha}\left(\frac{\pi}{2}\right)^{\beta}\frac{f^{\,\alpha-1}}{(f_{SW}/f)^{\beta-\alpha}}\ S \qquad (1.38).$$

Also, using eqs. 1.21, 1.35 and 1.36 one obtains the maximum value of the minor loop amplitude normalized to the sinusoidal induction amplitude:

$$\frac{\left|\Delta B_{ML_{\max}}\right|}{B_{S_m}} = \frac{\left|\Delta B\right]_{T_{SW}/2}\right|}{B_{S_m}} = \frac{\left|dB/dt\right| \left(T_{SW}/2\right)}{B_{S_m}} = \pi \; \frac{f}{f_{SW}} \qquad (1.39).$$

I - 3.4 *__Example:__ Typical values. Unipolar and bipolar comparison*

For typical values $\alpha = 1.3$, $\beta = 2.5$, $f_{SW} / f = 100$ and $f = 60 Hz$, eqs. 1.38 and 1.39 give:

$$\frac{p_{V_{ML}}}{p_{V_{Stm}}} = 0.0085 \qquad \text{and} \qquad \frac{\left|\Delta B_{ML_{\max}}\right|}{B_{S_m}} = 0.0031 \ .$$

For the same values but $f_{SW} / f = 20$ one obtains $\dfrac{p_{V_{ML}}}{p_{V_{Stm}}} = 0.0586$.

Therefore, for the most practical cases in bipolar PWM, the increase of losses due to minor loops may be neglected, and only the expression obtained for unipolar PWM (eq. E1.5) may be used for design purposes.

Notice that the actual voltage shape factor in bipolar PWM is $f_{fV} = 1$. Thus, a direct utilization of the actual voltage waveform in the eq. 1.18 (instead of the shape factor of the equivalent voltage waveform) will give wrong results, lower than the ones obtained from the classical Steinmetz equation. This is because, $\left|V\right|_{av} = \dfrac{2}{T}\int_0^{T/2} \left|v_{(t)}\right| \, dt = \dfrac{2}{T}\int_0^{T/2} v_{(t)} \, dt$ (which is only valid for unipolar waveforms), in the eq. 1.18 derivation.

On the other hand, substituting the actual induction vector in the ESE, without taking account of minor loops, yields values higher than the real ones. In such a case:

$$\dot{B}_{rms} = \left|\dot{B}\right|_{av} = \left|\frac{dB}{dt}\right| = \frac{\left|\Delta B_{ML_{\max}}\right|}{T_{SW}/2} = 2 \; f_{SW} \left|\Delta B_{ML_{\max}}\right| \qquad (1.40)$$

$$\Delta B = 2 \; B_{S_m} + \left|\Delta B_{ML_{\max}}\right| \qquad (1.41).$$

Substituting these values into the ESE expression (eq. 1.12) and dividing by the classical Steinmetz expression:

$$\frac{p_{V_{ML}}}{p_{V_{Stm}}} = \frac{1.234}{\left(4.863\right)^{\alpha}} \; \left(2\right)^{\alpha} \; \frac{1}{\left(\dfrac{1}{2} + \dfrac{B_{S_m}}{\left|\Delta B_{ML_{\max}}\right|}\right)^{\alpha}} \left(\frac{f_{SW}}{f}\right)^{\alpha} \qquad (1.42).$$

If $f_{SW} >> f$ then $B_{S_m} >> \left|\Delta B_{ML_{\max}}\right|$, and the eq. 1.42 becomes:

$$\frac{p_{V_{ML}}}{p_{V_{Stm}}} \cong \frac{1.234}{\left(4.863\right)^{\alpha}} \; \left(2\right)^{\alpha} \left(\frac{\left|\Delta B_{ML_{\max}}\right|}{B_{S_m}}\right)^{\alpha} \left(\frac{f_{SW}}{f}\right)^{\alpha} \qquad (1.43).$$

Substituting eq. 1.39 into eq. 1.43 yields:

$$\frac{p_{V_{ML}}}{p_{V_{Stm}}} \cong \frac{1.234}{\left(4.863\right)^{\alpha}} \; \left(2\,\pi\right)^{\alpha} = 1.234 \; \left(1.292\right)^{\alpha} \qquad (1.44).$$

For a typical value of $\alpha = 1.3$, eq. 1.44 gives: $\dfrac{p_{V_{ML}}}{p_{V_{Stm}}} = 1.722$, which is a value too high.

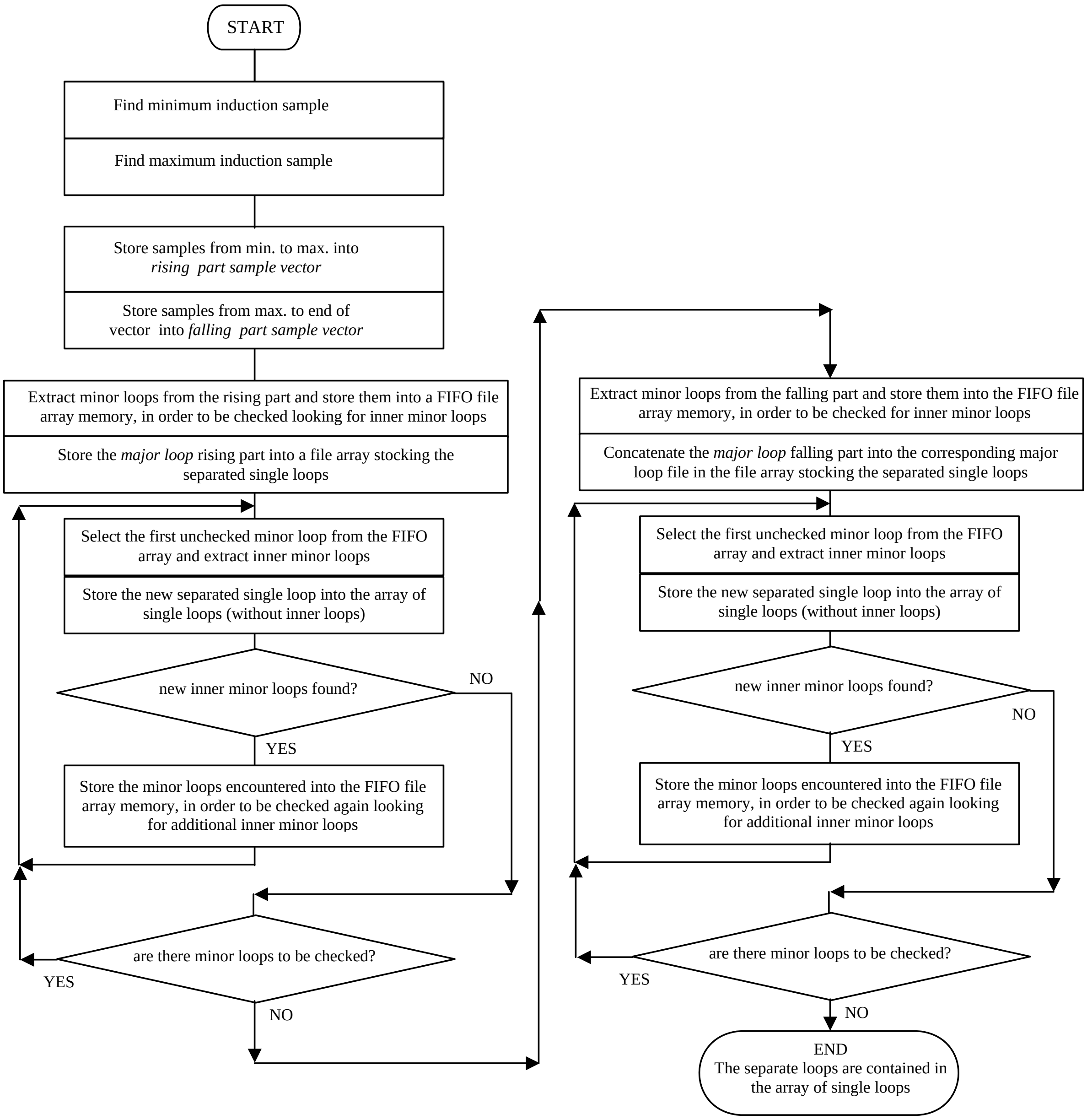

Fig. 1.8 : Flow chart of the function used for minor loop separation.

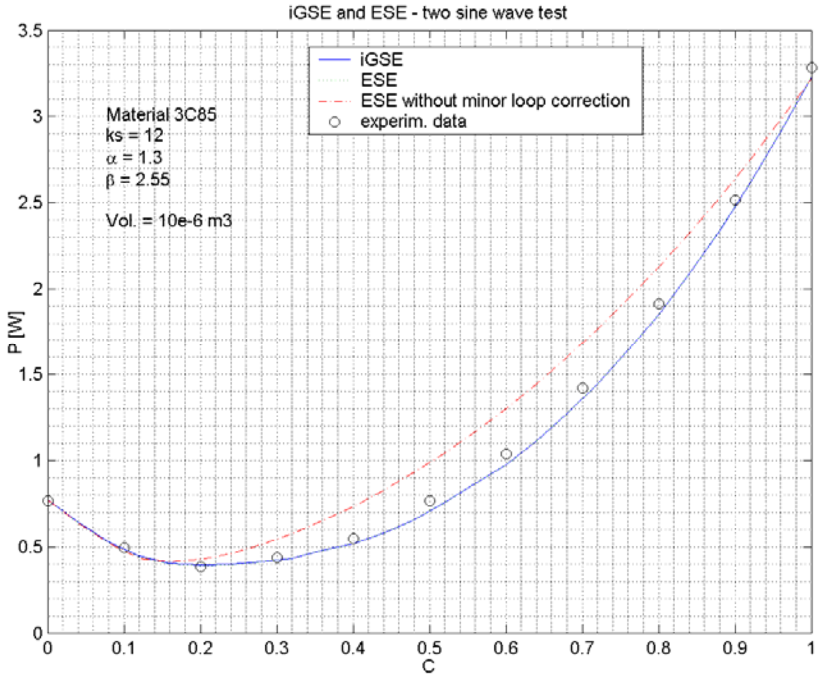

Fig. 1.9: Test using a sinewave adding variable third harmonic contents *"c"*.

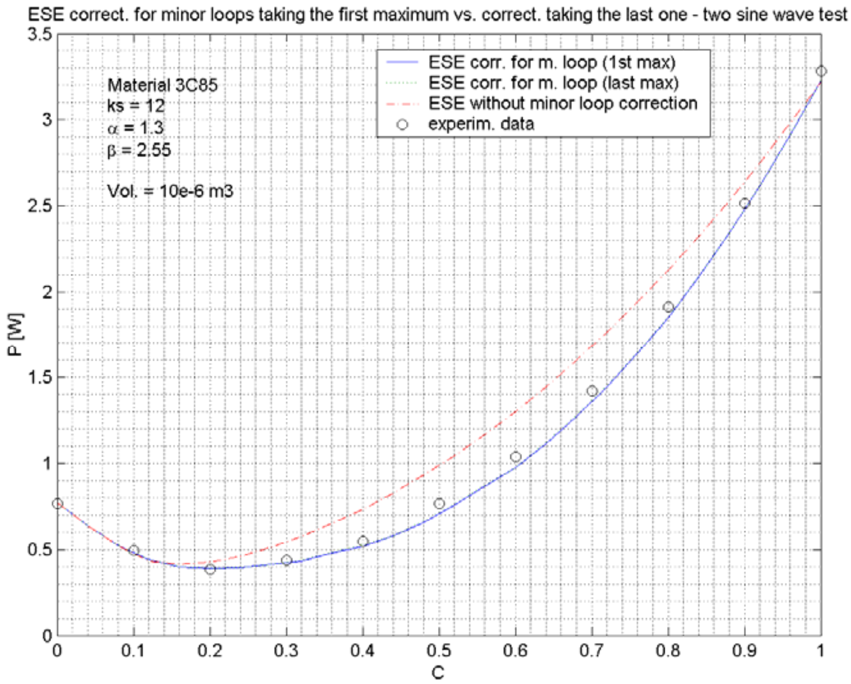

Fig. 1.10: Comparison of results using first maximum detection and last maximum detection in the minor loop separation algorithm in the test using a sinewave with variable third harmonic contents *"c"*.

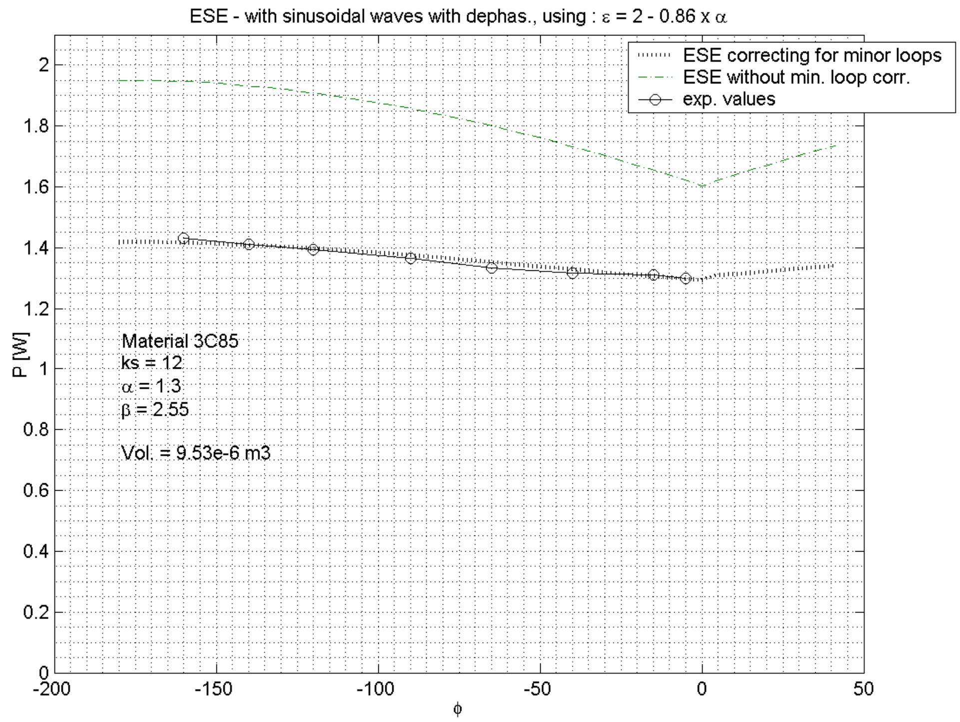

Fig. 1.11: Test using two added sinewaves with *c* = 0.7 and variable phase.

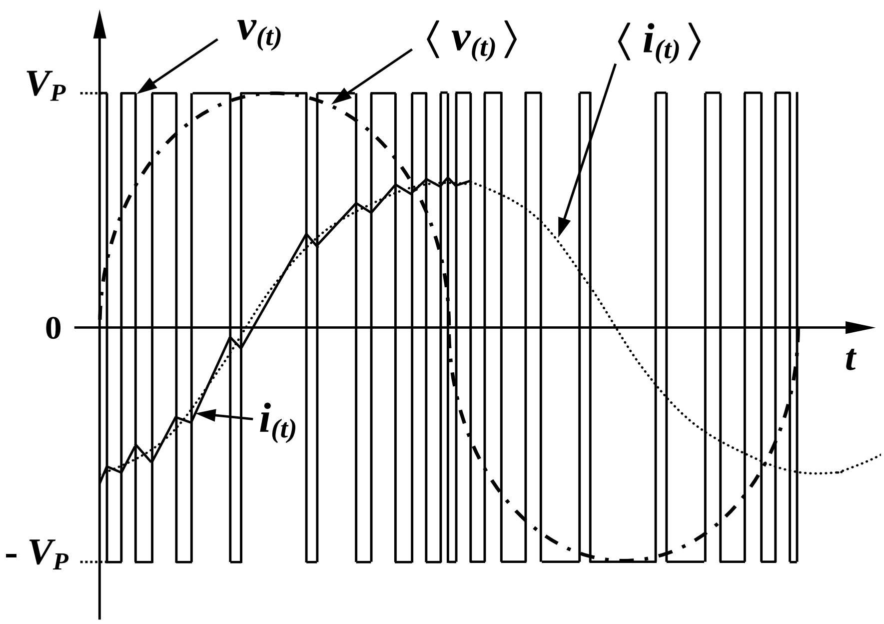

Fig. 1.12 : Bipolar PWM waveforms (local average values in dashed lines).

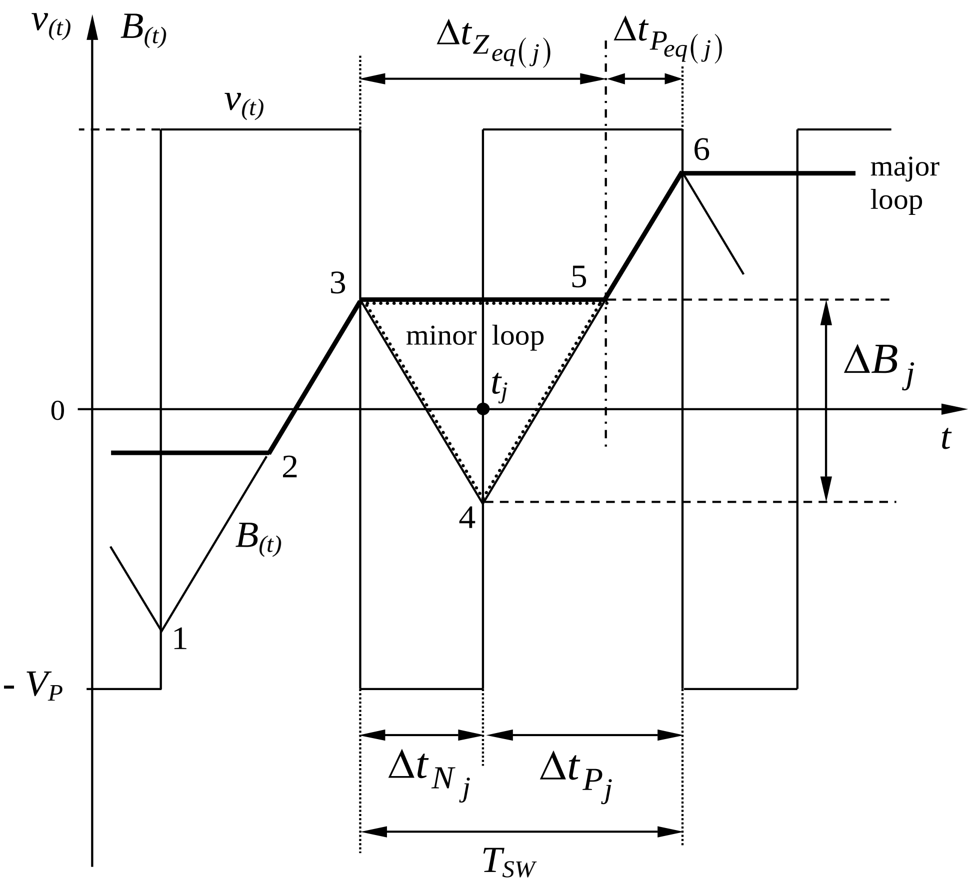

Fig. 1.13 : Switching-cycle detail in bipolar PWM waveforms.

I - 4. CONCLUSIONS

1) To design the magnetic components for symmetrical converters used in SMPS the classical Steinmetz equation is good enough because the duty cycle at nominal output power is usually chosen to be near the theoretical maximum in order to maximize the utilization of power transistors.

2) For the above applications the widely used adhoc criterion, adding harmonic power components to the basic Steinmetz equation results, is not justified for the typical duty cycles at nominal output power operation.

3) For $\alpha \cong 1.3$ eq. 1.18 yields a very simple approximate formula: $\dfrac{p_v}{p_{v_{Stm}}} \cong \sqrt{f_{f_V}} = \sqrt{\dfrac{V_{rms}}{|V|_{av}}}$ (1.45).

4) The fact that the classical Steinmetz is suitable for most practical cases in symmetrical converters, justifies the approximate expressions [4] for maximum induction adoption:

$$B_m\Big]_{opt} = \left[\frac{\frac{\Delta\theta}{R_{\theta_{tot}}} \Big/ \mathrm{Vol}_{Fe}}{k_s \;\; f^{\alpha} \left(1+\frac{\beta}{2}\right)} \right]^{1/\beta}$$ for optimum efficiency

and

$$B_m\Big]_{Po_{\max}} = B_m\Big]_{opt} \left[\left(\frac{S_{dis_{Fe}}}{S_{dis_{tot}}} \right) \left(1+\frac{\beta}{2}\right) \right]^{1/\beta}$$ for maximum output power density.

In these eqs. :

S_{dis} : heat dissipation surface

$\Delta\theta$: temperature rise over 40 ^{o}C

$R_{\theta_{tot}}$: thermal resistance

5) In bipolar PWM the minor loop contribution may be neglected when the carrier frequency is much higher than the fundamental one; only the major loop contribution is significant.

Usually, the power losses increase from 10 to 15 % with respect to those expected in an equivalent sinusoidal operation (having the same maximal induction).

REFERENCES

[1] W. Roshen, “Ferrite Core Loss for Power Magnetic Components Design”, *IEEE Trans. on Magnetics* , vol. 27, no. 6, Nov. 1991.

[2] J. Li, T. Abdallah, and C. R. Sullivan, “Improved Calculation of Core Loss with Nonsinusoidal Waveforms”, *IEEE Industry Applications Society Annual Meeting*, Oct. 2001, Chicago.

[3] K. Venkatachalam, C. R. Sullivan, T. Abdallah, and H. Tacca, “Accurate Prediction of Ferrite Core Loss with Nonsinusoidal Waveforms using Only Steinmetz Parameters”, *COMPEL 2002*, Jun. 2002, Puerto Rico.

[4] H.E. Tacca, “Flyback vs. Forward Converter Topology Comparison Based upon Magnetic Design”, *Eletrônica de Potência* , Vol. 5, no. 1, May 2000, Brazil.

APPENDIX A

MATLAB FUNCTIONS FOR MINOR LOOP SEPARATION

1. Function using first maximum detection

```
function [BSL,n]=seploop(B)
% main routine for loop separation
% input data : B= vector of induction,
% output data: BSL= cell array containing separated minor loops without inner minor loops, n=number of minor loops
% (This function calls the ancillary function : minloop)
BML=cell(1); %BML= cell array storing minor loops to process
BSL=cell(1);
j=1; % counter of loops without inner loops
k=1; % counter of loops to be checked for minor loop search
BML{1}=B; % array of loops to be processed for minor loop extraction
% Single loop extraction:
while j<=k
   Bi=BML{j};
   [BL,ML,m]=minloop(Bi);  % BL=vector cleaned of minor loops, ML= cell array containig minor loops extracted,
m=number of minor loops found.
   k=k+m; % increasing counter of loops to be processed
   BSL{j}=BL;
   j=j+1;
   if m>0
      BML=[BML ML]; % concatenation of additional loops to be checked for minor loop extraction
   end
end
n=j-1; % number of minor loops
```

```
function [BL,ML,m]=minloop(B)
% major loop separation from minor loops
% data input: B=induction,
% data output: BL= vector without minor loops, ML= cell array containing minor loops for further iterative processing,
m=number of loops extracted.
% INPUT DATA ARRANGING: single cycle definition, rising and falling part separation
T1=size(B);
T=T1(1,2); % period determination
B2T=[B B]; % input vector concatenation to obtain two cycles of data input signal
[Bmin,jmin]=min(B2T); % determination of rising part start point
B1T=B2T(jmin:jmin+T-1); % single cycle data extraction (1 cycle starting at start point)
[Bmax,jmax]=max(B1T); % determ. of end of rising part
Br=B1T(1:jmax); % rising part separation
Bf=B1T(jmax+1:end); % falling part separation
% RISING PART MINOR LOOP EXTRACTION:
% variable initialization:
m=0; % minor loop counter
flag=1; % set ancillary bit flag
ML=cell(1); % cell array definition and initialization
jfin1=size(Bf);
jfin=jfin1(1,2); % dimension of falling part
BL(1)=Br(1);
% rising part iterative minor loop extraction:
for j=1:jmax-1
```

```
    if (flag==1)
        if Br(j+1)>=Br(j)
            BL=[BL Br(j+1)]; % major loop accumulation
        else
            BC=Br(j); % BC=temporary comparation register
            jbc=j+1;  % minor loop starting point
            flag=0;   % reset flag
        end
    end
    if (flag==0)
        if (Br(j+1)>BC) % minor loop end point detection
            m=m+1;
            ML{m}=Br(jbc:j); % minor loop accumulation
            BL=[BL Br(j+1)]; % resume major loop accumulation
            flag=1;  % set flag
        end
    end
end
% FALLING PART MINOR LOOP EXTRACTION(similar to rising part extraction):
if jfin>0
    BL=[BL Bf(1)]; % variable initialization
    flag=1;
% falling part iterative minor loop extraction:
    if jfin>1 % detect if there are at least two samples in the falling part
        for j=1:jfin-1
            if (flag==1)
                if Bf(j+1)<=Bf(j)
                    BL=[BL Bf(j+1)];
                else
                    BC=Bf(j);
                    jbc=j+1;
                    flag=0;
                end
            end
            if (flag==0)
                if (Bf(j+1)<BC) % minor loop end point detection
                    m=m+1;
                    ML{m}=Bf(jbc:j); % minor loop accumulation
                    BL=[BL Bf(j+1)]; % resume major loop accumulation
                    flag=1;
                    else if (j==jfin-1) % end of loop detection
                            m=m+1;
                            ML{m}=Bf(jbc:jfin); % minor loop accumulation
                    end
                end
            end
        end
    end
end
```

---

2. Function using last maximum detection

```
function [BSL,n]=seploopf(B)
% main routine for loop separation
% input data : B= vector of induction,
% output data: BSL= cell array containing separated minor loops without inner minor loops, n=number of minor loops
```

```
% (This function calls the ancillary function : minloop)
BML=cell(1); %BML= cell array storing minor loops to process
BSL=cell(1);
j=1; % counter of loops without inner loops
k=1; % counter of loops to be checked for minor loop search
BML{1}=B; % array of loops to be processed for minor loop extraction
% Single loop extraction:
while j<=k
   Bi=BML{j};
   [BL,ML,m]=minloopf(Bi);  % BL=vector cleaned of minor loops, ML= cell array containig minor loops extracted,
m=number of minor loops found.
   k=k+m; % increasing counter of loops to be processed
   BSL{j}=BL;
   j=j+1;
   if m>0
      BML=[BML ML]; % concatenation of additional loops to be checked for minor loop extraction
   end
end
n=j-1; % number of minor loops
```

```
function [BL,ML,m]=minloopf(B)
% major loop separation from minor loops
% data input: B=induction,
% data output: BL= vector without minor loops, ML= cell array containing minor loops for further iterative processing,
m=number of loops extracted.
% INPUT DATA ARRANGING: single cycle definition, rising and falling part separation
T1=size(B);
T=T1(1,2); % period determination
B2T=[B B]; % input vector concatenation to obtain two cycles of data input signal
[Bmin,jmin]=min(B2T); % determination of rising part start point
B1T=B2T(jmin:jmin+T-1); % single cycle data extraction (1 cycle starting at start point)
BX=fliplr(B1T);% invert B1T to obtain the last maximum
[Bmax,jx]=max(BX); % last maximum detection
jmax= T+1-jx; % determ. of end of rising part
Br=B1T(1:jmax); % rising part separation
Bf=B1T(jmax+1:end); % falling part separation
% RISING PART MINOR LOOP EXTRACTION:
% variable initialization:
m=0; % minor loop counter
flag=1; % set ancillary bit flag
ML=cell(1); % cell array definition and initialization
jfin1=size(Bf);
jfin=jfin1(1,2); % dimension of falling part
BL(1)=Br(1);
% rising part iterative minor loop extraction:
for j=1:jmax-1
   if (flag==1)
      if Br(j+1)>=Br(j)
         BL=[BL Br(j+1)]; % major loop accumulation
      else
         BC=Br(j); % BC=temporary comparation register
         jbc=j+1;  % minor loop starting point
         flag=0;   % reset flag
      end
   end
   if (flag==0)
```

```
        if (Br(j+1)>BC) % minor loop end point detection
            m=m+1;
            ML{m}=Br(jbc:j); % minor loop accumulation
            BL=[BL Br(j+1)]; % resume major loop accumulation
            flag=1;  % set flag
            else if (j==jmax-1) % end of minor loop detection
                     m=m+1;
                     ML{m}=Br(jbc:jmax); % minor loop accumulation
                     flag=1;  % set flag
            end
        end
    end
end
% FALLING PART MINOR LOOP EXTRACTION(similar to rising part extraction):
if jfin>0
    BL=[BL Bf(1)]; % variable initialization
    flag=1;
% falling part iterative minor loop extraction:
    if jfin>1 % detect if there are at least two samples in the falling part
        for j=1:jfin-1
            if (flag==1)
                if Bf(j+1)<=Bf(j)
                    BL=[BL Bf(j+1)];
                else
                    BC=Bf(j);
                    jbc=j+1;
                    flag=0;
                end
            end
            if (flag==0)
                if (Bf(j+1)<BC) % minor loop end point detection
                    m=m+1;
                    ML{m}=Bf(jbc:j); % minor loop accumulation
                    BL=[BL Bf(j+1)]; % resume major loop accumulation
                    flag=1;
                    else if (j==jfin-1) % end of loop detection
                            m=m+1;
                            ML{m}=Bf(jbc:jfin); % minor loop accumulation
                    end
                end
            end
        end
    end
end
```

PART II

CONSIDERING DC-BIAS EFFECTS ON MAGNETIC LOSSES WITH THE EXTENDED STEINMETZ EQUATION (ESE)

II - CONSIDERING DC-BIAS EFFECTS ON MAGNETIC LOSSES WITH THE EXTENDED STEINMETZ EQUATION (ESE)

II - 1. MODEL DEVELOPMENT

II - 1.1 *Modeling principles*

In [1], in order to take account of the dc bias, the losses obtained from the Steinmetz equation are increased multiplying by a factor :

$$M = 1 + K_1 \, B_{DC} \, e^{-\frac{B_{AC}}{K_2}} \tag{2.1}$$

where B_{DC} and B_{AC} relate to the constant and the alternating part of the induction, while K_1 and K_2 must be determined from measurements.

Because the dc bias influence becomes stronger as the saturation level is approached, normalization to this level should be introduced. In addition, experimental curves show that the dc bias influence is not linear, so better fitting with experimental data would be obtained by affecting the bias induction by an exponent.

Therefore, the former model may be modified multiplying the ESE by a factor:

$$M = 1 + \kappa \left(\frac{|B_{DC}|}{B_{SAT}} \right)^{\nu} e^{-\xi \frac{\Delta B/2}{B_{SAT}}} \tag{2.2}$$

where,

ΔB	is the equivalent amplitude of the induction to be introduced in ESE, given by the algorithm taking account for multiple minor loops influence (deducting the DC bias),
B_{DC}	is the dc bias induction,
B_{SAT}	is the saturation induction,
κ , ν , ξ	are constants depending on the ferrite material.

The constant ν seems not having a critical value and good fitting for different materials is obtained adopting $\nu = 1.6$.

From experimental values, the constant ξ might be expressed as:

$$\xi = (16/\kappa)^2 \tag{2.3}$$

Experimental work has to be done in order to prove this relation and to determine if some relation exist between these constants and the Steinmetz equation parameters.

II - 1.2 *Comparison against experimental results*

The modified version of ESE, considering the M factor, is compared against experimental data from [2] to test its fitting capabilities.

Fig. 2.1 shows the ESE results obtained for a biased sine wave applied to a core made of 3F3 ferrite, while Fig.2.2 shows curves for N27 material.

The sine wave frequency used in Figs 2.1 and 2.2 was 20kHz [2].

Fig. 2.3 shows the frequency related variation of losses depending upon dc bias and ac driving. The deviation from the experimental results presented in [2] is probably due to a mismatch between the real physical law of losses and the approximative Steinmetz expression (because unavoidable differences arise even at zero biasing level).

II - 2. SIMPLIFIED MODELS

The exponential function in eq. 2.2 would complicate the application to asymmetrical converters. Moreover, a model including fewer parameters should be preferable.

Therefore, the exponential term is roughly substituted by a linear function yielding:

$$M = 1 + K_{dc} \left(\frac{|B_{DC}|}{B_{SAT}} \right)^{\Lambda} \left(1 - \Xi \frac{\Delta B}{B_{SAT}} \right) \qquad (2.4).$$

The constants K_{dc} , Λ and Ξ are determined by looking for the best fitting with experimental values.

The Figs. 2.4 and 2.5 show acceptable agreement between the above used experimental values and the new results from the proposed simplified model. For the different materials considered, acceptable experimental data matching is achieved adopting $\Lambda = 2$ and $\Xi = 1$, while K_{dc} depends on the material type and must be determined looking for the best experimental curve matching.

Substituting for the constant values in eq. 2.4 , one obtains :

$$M = 1 + K_{dc} \left(\frac{|B_{DC}|}{B_{SAT}} \right)^{2} \left(1 - \frac{\Delta B}{B_{SAT}} \right) \qquad (2.5).$$

The problem with this model is that one may expect that the amplitude of the ac component could be of the same order of the saturation level when the dc component is small, and in such a case a value of *M* lower than one will result, which would be incorrect.

To overcome this problem another approximation to the exponential function is used, leading to the model:

$$M = 1 + \kappa \left(\frac{|B_{DC}|}{B_{SAT}} \right)^{\nu} \left(\frac{1}{1 + \zeta \left(\frac{\Delta B/2}{B_{SAT}} \right)^{2}} \right) \qquad (2.6).$$

In this model, the constants κ , ν are the same as in the first model (using the exponential function), while ζ has to be found experimentally. For the materials explored, it is found that adopting $\zeta = 2\,\xi^2$ and using eq. 2.3 yields

$$\zeta = 2 \left(\frac{16}{\kappa} \right)^{4} \qquad (2.7)$$

which, substituted in eq. 2.6, gives good approximated results:

$$M = 1 + \kappa \left(\frac{|B_{DC}|}{B_{SAT}} \right)^{1.6} \left(\frac{1}{1 + 2 \left(\frac{16}{\kappa} \right)^{4} \left(\frac{\Delta B/2}{B_{SAT}} \right)^{2}} \right) \qquad (2.8).$$

The curves obtained using eq. 2.8 are practically identical to those plotted in Figs. 2.1 and 2.2 .

The proposed models do not take account of the small loss reduction obtained when a slight dc bias is applied [3], nor are they valid for all ferrite set of Steinmetz parameters. In particular, for near zero induction operation the models do not represent even the shape of the losses' curves [3].

The simplest model has been tested using experimental data from two materials having quite different parameters[2]. Even though the agreement is good, further experimental verification should be done.

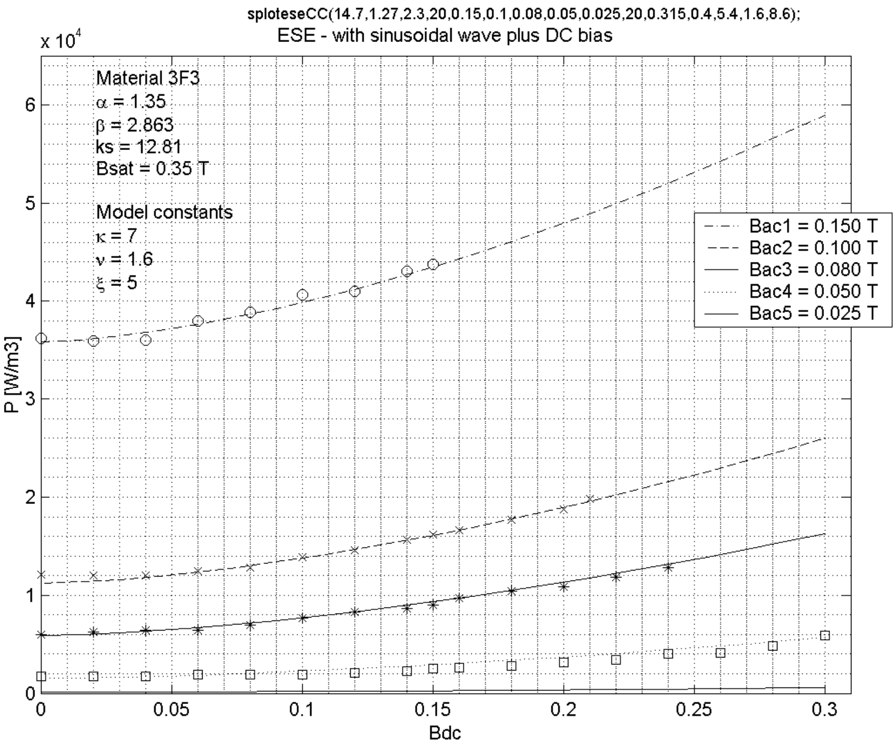

Fig. 2.1 : Loss density ESE plot considering dc bias, for a 3F3 ferrite made core.

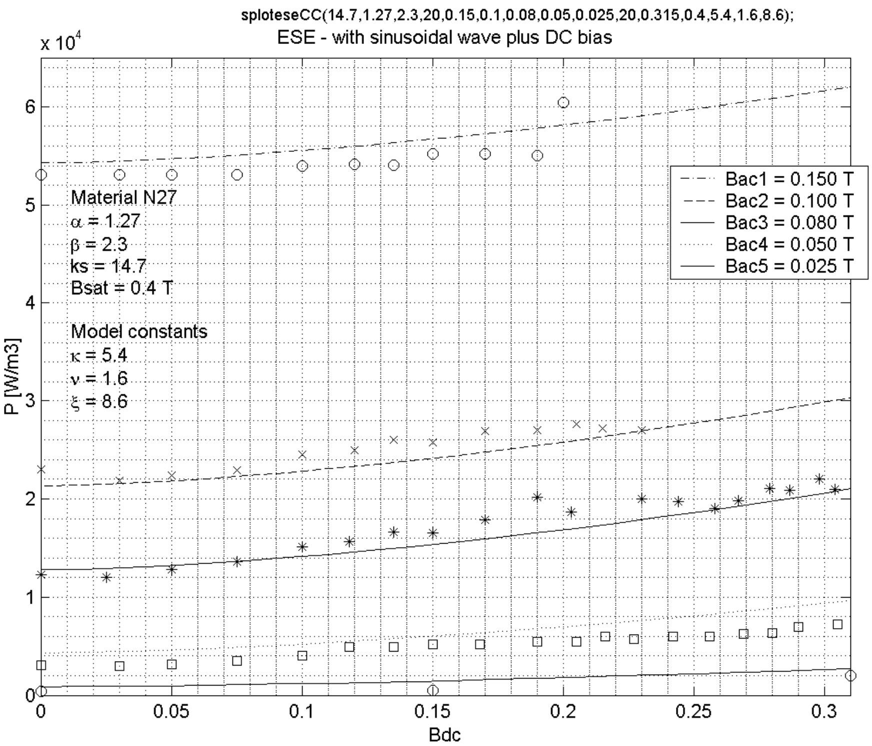

Fig. 2.2 : Loss density ESE plot considering dc bias, for a N27 ferrite made core.

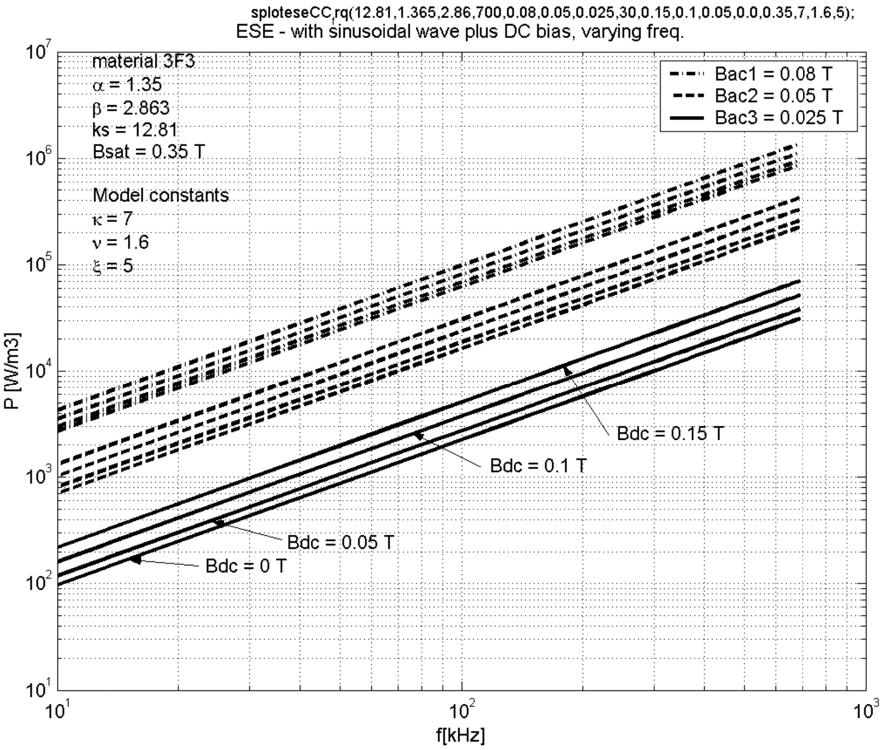

(a)

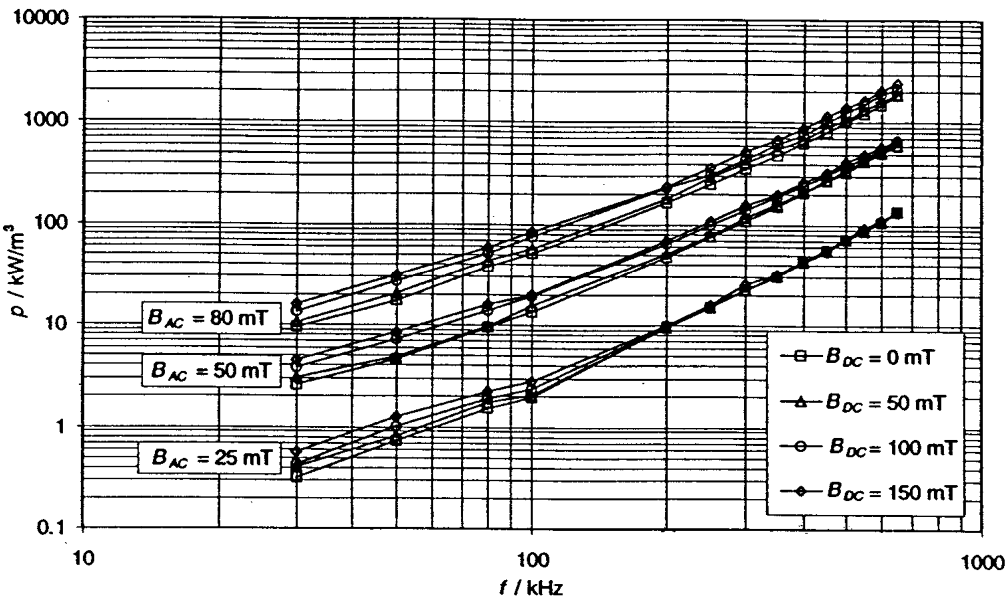

(b)

Fig. 2.3 : Loss density as function of frequency, considering dc bias, for a 3F3 ferrite made core, *(a)* results from eq. 2.2 , *(b)* experimental values from [2].

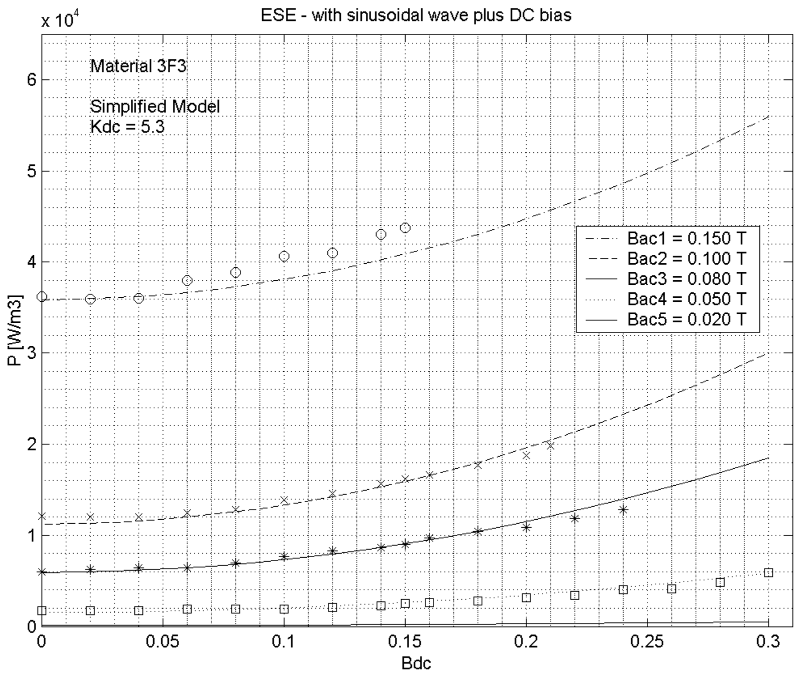

Fig. 2.4 : Loss density ESE plot considering dc bias, for a 3F3 ferrite made core, using the linear simplified model.

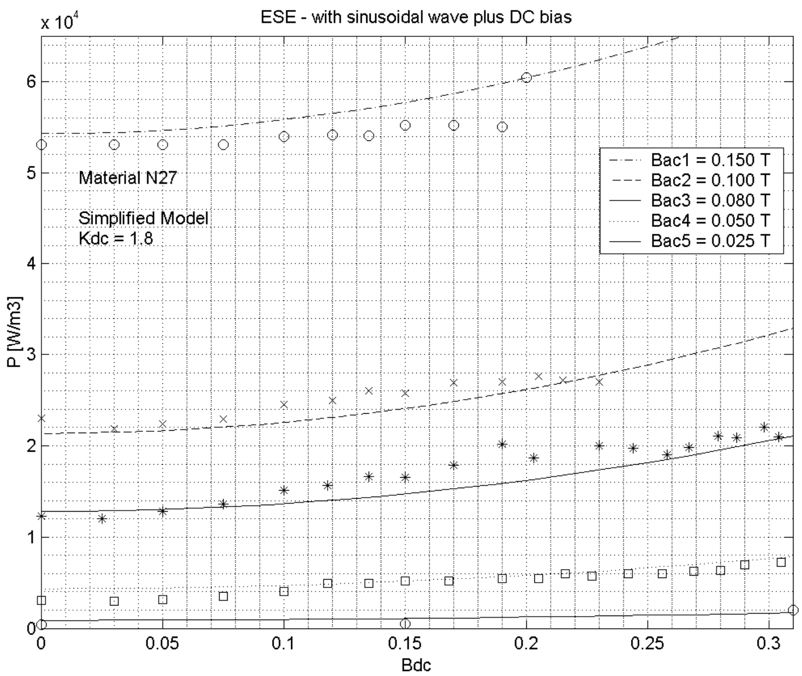

Fig. 2.5 : Loss density ESE plot considering dc bias, for a 3F3 ferrite made core, using the linear simplified model.

II - 3. ***Example:***

Application to a flyback converter operating in continuous mode

The characteristic waveforms are shown in Fig. 2.6.
Considering the dc bias the ESE may expressed as:

$$\frac{p_v}{p_{v_{Stm}}} = 1.234\,(0.82254)^{\alpha}\,\left(f_{f_V}\right)^{(1.86\,\alpha\,-\,2)}\,M \tag{2.9}$$

where f_{f_V} is the shape factor of the primary voltage and M is the dc bias loss multiplication factor previously defined.

In continuous mode, $V_S = \frac{n_P}{n_S}\frac{D}{1-D}V_P$, then:

$$f_{f_V} = \frac{V_{P\,rms}}{\left|V_P\right|_{av}} = \frac{1}{2\sqrt{D(1-D)}} \tag{2.10}$$

On the other hand, from the Ampère law:

$$mmf_{(t)} = n_P\; i_{P(t)} = B_{(t)}\,\frac{l_{Fe}}{\mu_o\;\mu_{r_e}} \tag{2.11}$$

which yields,

$$mmf_{\max} = n_P\; I_{P\max} = B_m\,\frac{l_{Fe}}{\mu_o\;\mu_{r_e}} \tag{2.12}$$

$$mmf_{av} = \frac{n_P}{2}\left(I_{P\max} + I_{P\min}\right) = B_{av}\,\frac{l_{Fe}}{\mu_o\;\mu_{r_e}} = B_{DC}\,\frac{l_{Fe}}{\mu_o\;\mu_{r_e}} \tag{2.13}$$

$$\Delta mmf = n_P\;\Delta I_P = \Delta B\,\frac{l_{Fe}}{\mu_o\;\mu_{r_e}} \tag{2.14}$$

From eqs. 2.12 and 2.14, one obtains:

$$\frac{\Delta B}{B_m} = \frac{\Delta I_P}{I_{P\max}} = \delta_i \tag{2.15}$$

where δ_i is a parameter used in converter design [4].

Therefore:

$$\frac{\Delta B}{B_{SAT}} = \frac{\Delta B}{B_m}\,\frac{B_m}{B_{SAT}} = \delta_i\,\frac{B_m}{B_{SAT}} \tag{2.16}$$

In similar way, from eqs. 2.12 and 2.13 we can obtain:

$$\frac{B_{DC}}{B_m} = \left(1 - \frac{\delta_i}{2}\right) \tag{2.17}$$

and then,

$$\frac{\left|B_{DC}\right|}{B_{SAT}} = \frac{\left|B_{DC}\right|}{B_m}\,\frac{B_m}{B_{SAT}} = \left(1 - \frac{\delta_i}{2}\right)\frac{B_m}{B_{SAT}} \tag{2.18}$$

Substituting eqs. 2.16 and 2.18 into 2.2 yields:

$$M = 1 + \kappa \left(1 - \frac{\delta_i}{2}\right)^{\nu} \left(\frac{B_m}{B_{SAT}}\right)^{\nu} e^{-\xi \left(\frac{\delta_i}{2}\right) \frac{B_m}{B_{SAT}}} \quad (2.19).$$

Substituting eqs. 2.10 and 2.19 into 2.9 yields:

$$\frac{p_v}{p_{v_{Stm}}} = 1.234 \frac{(0.82254)^{\alpha}}{\left[2\sqrt{D(1-D)}\right]^{(1.86\,\alpha-2)}} \left[1 + \kappa \left(1 - \frac{\delta_i}{2}\right)^{\nu} \left(\frac{B_m}{B_{SAT}}\right)^{\nu} e^{-\xi \left(\frac{\delta_i}{2}\right) \frac{B_m}{B_{SAT}}}\right] \quad (2.20).$$

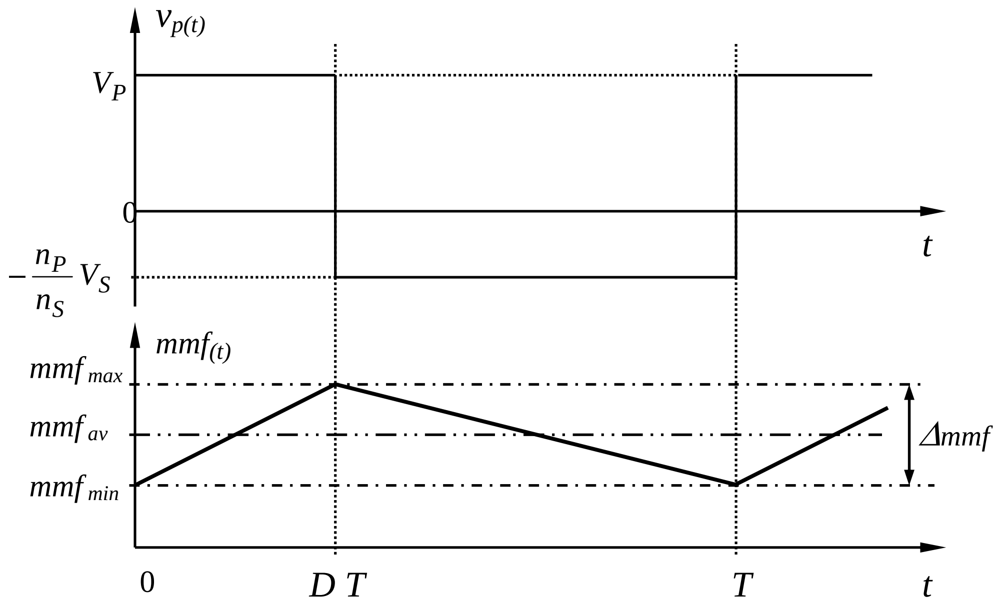

Fig. 2.6 : Continuous operating mode flyback waveforms.

For a set of typical values $D = 0.5$, $\alpha = 1.35$, $B_m \cong B_{SAT}$, $\delta_i = 1/3$, $\kappa = 7$, $\nu = 1.6$ and $\xi = 5$, one obtains: $\frac{p_v}{p_{v_{Stm}}} = 3.1$, but in this expression $p_{v_{Stm}}$ corresponds to losses obtained for $\Delta B = \delta_i \; B_{SAT}$, and so is quite small compared to the losses in a transformer operating with $\Delta B = 2 \; B_m$.

REFERENCES

[1] J.Reinert, A. Brockmeyer, and R.W. A. A. De Doncker, “Calculation of Losses in Ferro- and Ferrimagnetic Materials Based on the Modified Steinmetz Equation”, *IEEE Transactions on Industry Applications*, vol. 37, no. 4, Jul./Aug. 2001.

[2] A. Brockmeyer, “Dimensionerungswerkzeug für magnetische Bauelemente in Stromritchteranwendungen”, Ph.D. dissertation, Inst. Power Electron., Aachen, Germany, 1997.

[3] W. K. Mo, D. K. W. Cheng, and Y. S. Lee, “Simple Approximations of the DC Flux Influence on the Core Loss Power Electronic Ferrites and Their Use in Design of Magnetic Components”, *IEEE Transactions on Industrial Electronics*, vol.44, no. 6, Dec. 1997.

[4] H.E. Tacca, “Flyback vs. Forward Converter Topology Comparison Based upon Magnetic Design”, *Eletrônica de Potência* , Vol. 5, no. 1, May 2000, Brazil.

PART III

MEASUREMENT TECHNIQUES

III - MEASUREMENT TECHNIQUES. PRINCIPLES

Electrical measurement methods are faster than the thermal ones.

Therefore, due to the big amount of measurements to be done, the core loss will be measured by electrical methods, based upon the basic approach introduced by Epstein (Fig. 3.1) [1].

In order to calculate the power loss, a digital oscilloscope does the multiplication and integration of the voltage and current signals.

A high inductance inductor is inserted in the dc biasing circuit to reduce ac power losses in the dc circuit.

The switch S_{dc} in position 1 avoids dc current circulation through the current sense transformer, but some error could be introduced due to losses in the biasing circuit. In position 2 this losses are not sensed, but a dc current circulates through the current transformer, enabling the possibility of errors if the transformer core approaches the saturation limit.

Depending upon the dc bias and the current transformer features, one of both alternatives should be preferred.

The cores to be utilized need to have a constant section to ensure that the induction be uniform (this leads to discard some popular shapes widely used in power conversion). In fact, only toroids and some E cores fulfill this requirement.

The static curves of ferrites exhibit wide dispersion among different samples. So, one way to set accurately the dc bias induction is to prevent dc bias depending on the material characteristics. To achieve this, an air gap large enough, should be inserted into the magnetic circuit. This may be done adopting E cores or cutting toroids.

The other alternative is to adopt non-gapped cores, but measuring the actual static curves of the samples to be used in measurements.

In following sections, both alternatives are considered.

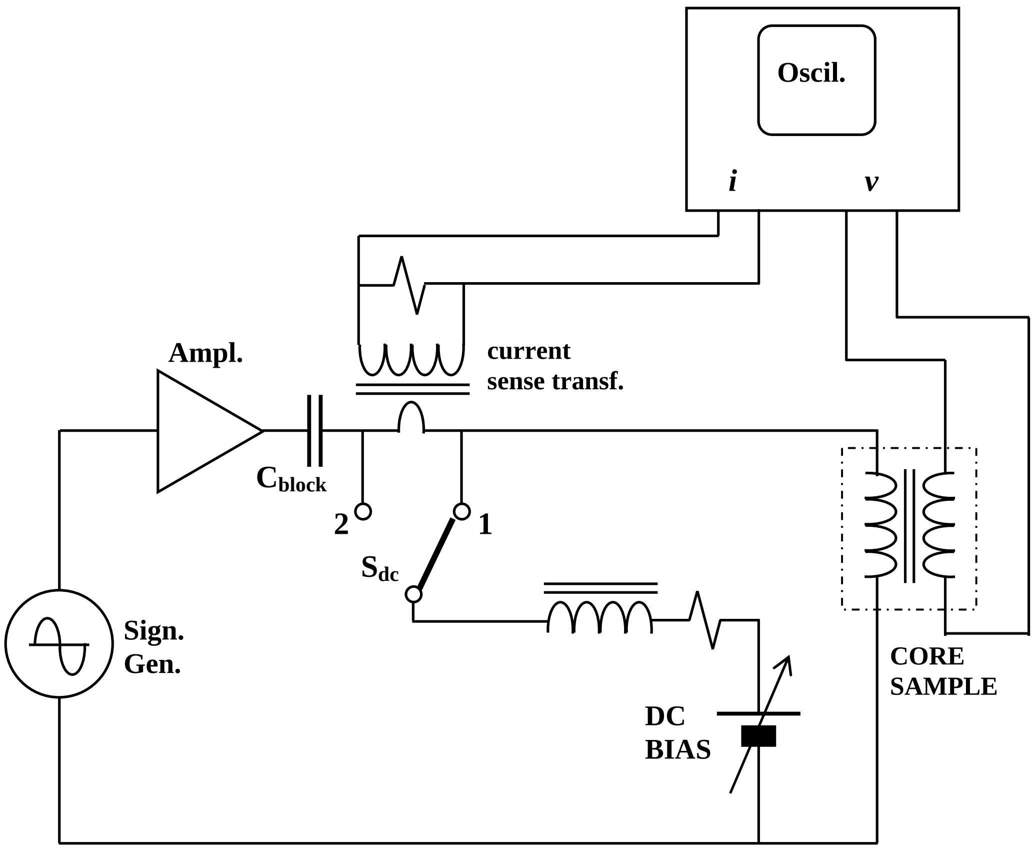

Fig. 3.1 : Basic core loss measurement circuit.

<u>REMARK</u>: As the ferrite characteristics depend on the material temperature, the core samples under test are immersed in a bath of transformer oil heated at 100 ^{o}C.

III - 1. MEASUREMENTS USING GAPPED CORES

Non-gapped E standard cores will be adopted and the air gap will be inserted in the central and side legs using paper.

If the required air gap does not match any of the ones specified in manufacturer data sheets, the effective permeability and inductance factor may be estimated using the formula presented in Appendix B.

Once the air gap is adopted, it is advisable to verify these calculated values before doing the experimental measurements.

III - 1.1 *Selection of the core volume*

If the air gap fulfills $l_a >> l_e / \mu_r$, the effective permeability becomes:

$$\mu_{r_e} = \frac{\mu_r}{1 + \mu_r \dfrac{l_a}{l_e}} \cong l_e / l_a \qquad (3.1).$$

Then, adopting: $l_a = 20 \left(le / \mu_{r_{\min}} \right)$, one obtains: $\mu_{r_e} = \mu_{r_{\min}} / 20 \cong 100$.

For the ferrite material 3C85 at 100 ^{o}C, from manufacturer data it is, $\mu_{r_{\min}} = 2000$ and $\mu_{r_{\max}} = 4400$.

Therefore, this yields:

$\mu_{r_{e\,\min}} = 95.23$, $\mu_{r_{e\,\max}} = 97.78$ and $\mu_{r_{e\,av}} = 96.51$.

Thus, the error due to relative permeability variation during measurements could be:

$e_{\mu r} = \dfrac{\mu_{r_{e\,\max}} - \mu_{r_{e\,\min}}}{\mu_{r_{e\,av}}} = 0.0264$, that is less than 3 %.

Therefore, air gaps yielding effective permeabilities of 100 (or less) should be adopted in order to keep the error small.

On the other hand, from the Ampère law:

$$I_m = \frac{B_m \; S_{Fe}}{A_L \; N} \qquad (3.2)$$

where,

$$A_L = \frac{\mu_o \; \mu_{r_e} \; S_{Fe}}{l_e} \qquad (3.3)$$

and from the Faraday law:

$$N = \frac{V_P}{4.44 \; B_m \; S_{Fe} \; f} \qquad (3.4).$$

Substituting eqs. 3.3 and 3.4 into eq. 3.2 yields:

$$I_m = \frac{4.44 \; B_m{}^2 \; Vol \; f}{\mu_o \; \mu_{r_e} \; V_P} \qquad (3.5)$$

where, $Vol = S_{Fe}\ l_e$.

From eq. 3.5 one may obtains the required core volume as function of the maximum current to be supplied by the driving amplifier:

$$Vol = \frac{\mu_o\ \mu_{r_e}\ V_P\ I_m}{4.44\ B_m^{\ 2}\ f} \qquad (3.6).$$

Considering $I_m = \sqrt{2}\, I$, the eq. 3.6 becomes:

$$Vol = \frac{\mu_o\ \mu_{r_e}\ P_{amp}}{\pi\ B_m^{\ 2}\ f} \qquad (3.7)$$

where P_{amp} is the required amplifier nominal output power.

Examples

For f = 20 kHz , B_m = 0.3 T , $\mu_{r_e} = 100$ and $P_{amp} = 250\,W$, it results: $Vol = 5555\ \text{mm}^3$.

The core E42/21/15 has a volume of 17300 mm^3 , so it is too big for the amplifier power available. This may be also verified using eqs. 3.2 and 3.4:

1. From eq. 3.4 : $N = 21.09 \cong 21$.

2. From manufacturer data one may adopt $\mu_{r_e} = 110$ which yields $A_L = 250\,\text{nH}$. Then, adopting $V_P = 100$ V , eq. 3.2 yields: $I_m = \dfrac{B_m\ S_{Fe}}{A_L\ N} = \dfrac{0.3 \times 178\ \ 10^{-6}}{250\ \ 10^{-9} \times 21}\ A = 10.17\ A$.

If an error of 5 % were acceptable, one may adopt $\mu_{r_e} = 270$, giving $A_L = 630\,\text{nH}$ which yields $I_m = 4$ A .

For f = 100 kHz, one may raise the induction up to B_m = 0.2 T and then, from eq. 3.4 : $N = 6.326 \cong 6$. Later, adopting $\mu_{r_e} = 270$ the eq. 3.2 yields: $I_m = 9.42$ A .

From results above obtained from eq. 3.7 , one possibility to measure the losses using the available amplifier of 250 W, might be to adopt cores EF25 (E25/13/7) having $Vol = 2990\ \text{mm}^3$.

This was the core size adopted to do the experimental measurements.

III - 1.2 *Minimum required window filling factor*

The rms current through the windings is:

$$I_{rms} = \frac{1}{\sqrt{2}} \frac{B_m\ S_{Fe}}{A_L\ N} \qquad (3.8).$$

On the other hand:

$$I_{rms} = \sigma\ S_{Cu} = \sigma\ F_p\ \ F_c\ \ F_w\ \frac{S_{Fe}}{N} \qquad (3.9)$$

where,

σ : current density

F_p : partition factor of the window

F_c : coil factor (or filling factor)

F_w : window factor , $F_w = S_w / S_{Fe}$

Substituting eq. 3.9 into eq. 3.8 yields:

$$F_{c_{\min}} = \frac{1}{\sqrt{2}} \frac{B_m}{A_L} \frac{1}{\sigma\, F_w\, F_p} \quad (3.10).$$

Thus , the filling factor should be equal or better than the limit given by eq. 3.10 .

For the cores E25/13/7 made with material 3C85, from manufacturer data the air gap should be 270 μm in order to set A_L with accuracy + - 3 % . Adopting such air gap (but sharing it between the external and central legs), it results $A_L = 240 \pm 3.1\,\%$.

For $B_m = 0.3\,T$, $\sigma = 4.5\; A/mm^2$, $F_w = 1.077$, and $F_p = 0.9$ the minimum filling factor results: $F_{c_{\min}} = 0.203$. This requirement may not be fulfilled using cable winding, because the window filling factor using cable typically ranges from 0.07 to 0.09 .

Using other cores the situation does not change much. For example , for E42-15 the minimum filling factor is 0.155 .

For a core E55-21, adopting $\sigma = 4.5\; A/mm^2$ and $F_p = 0.95$, it results $F_{c_{\min}} = 0.9$. Then, from eq. 3.8 it should be $I_{rms} = 3.96\; A$, but for this current and an environment temperature of 100 ^{o}C, it may be not safe to adopt such current density. (Lowering the current density will raise the minimum required filling factor).

Therefore, wire windings should be used. Moreover, the amount of winding space required will not allow to use isolated windings for ac driving primary and dc biasing windings.

III - 1.3 *Instrument accuracy requirements*

The averaged product of signals from channels 1 and 2 has usually an offset, which may change with the repetition of the measurement and with the number of averaging cycles. Also, it varies when the voltage/division rate is modified.

However, a simple way to correct for offset errors is to do two measurements (W_1 and W_2), inverting the connection of the voltage sense winding without changing the voltage/div ratios. As the offset error should remain the same, the expression $W = (W_1 - W_2)/2$ allows eliminating offset errors.

Unfortunately, this did not solve the accuracy problems.

Using a non-gapped core E25/13/7 made on material 3C85 , adopting Bm = 0.2 T and f = 25 kHz , the apparent power was 0.705 W , while the active power was 35 mW. That is, the ratio of the wanted average to the apparent instantaneous power to be averaged was FP = 0.05 (the power factor).

On the other hand, in the case of the gapped core, the power factor results: FP = 0.0045, so one order of magnitude lower.

Then to have a precision of $\pm 2.5\ \%$ on the result, a resolution of FP/40 in the signal product is required, that is FP/40 = 0.0001125 , which leads to a required precision of $\sqrt{FP/40} = 0.0106$ for the input signals. As the input signals may be usually ranging on the medium voltage span (selected by the voltage/div control) this ask for a 0.5 % class requirement for the input channels.

Moreover, the signal multiplication must have a 0.0001 resolution, which implies 14 bits. Actually, for signals ranging on the medium voltage span, the required resolution is 0.00005. Therefore, two bytes operation and register are needed.

Increasing the core volume, or using multiple cores in parallel, will not change the situation because the apparent power would be increased in the same proportion (both the active power and the apparent power are proportional to the core volume).

When using a non-gapped core the precision required becomes much lower due to the apparent power reduction.

If curves corresponding to small loss operation are to be plotted, the instrument accuracy demands may be impossible to meet when using gapped cores [2].

III - 2. MEASUREMENTS USING NON-GAPPED CORES

In ferrites the static B-H curve matches the low frequency normal curve [3] which allows to use this normal curve to find the dc currents to be injected.

Using a non-gapped core, for a given induction Bm it will be a maximum Hm related to a peak current Im by the Ampère law.

Assuming the normal curve equal to the static one, injecting Idc = Im should produce Bdc = Bm.

Therefore, to find the dc current to be injected one should apply an ac voltage producing a Bm equal to the desired Bdc , then measure Im and so finally inject Idc = Im.

The normal curve differs from the static curve as much as the core eddy currents become important. Thus, to obtain a good Idc prediction, one should use a low frequency normal curve, for example at 1 kHz.

This may be accomplished using two sets of windings, one having more turns to find Idc and other with few turns to measure losses.

In order to avoid resonance problems while doing high frequency measurements, a set of two coil formers should be foresee.

III - 2.1 *Normal curve measurement*

The core size adopted is E25/13/7 that has a volume big enough to have losses high enough to be measured with an accuracy of +- 9 % in worst cases.

The normal curves were obtained using the circuit of Fig. 3.2, with a coil former having primary and secondary windings of 50 turns bifilar wound.

All the measures were done at 100 ^{o}C.

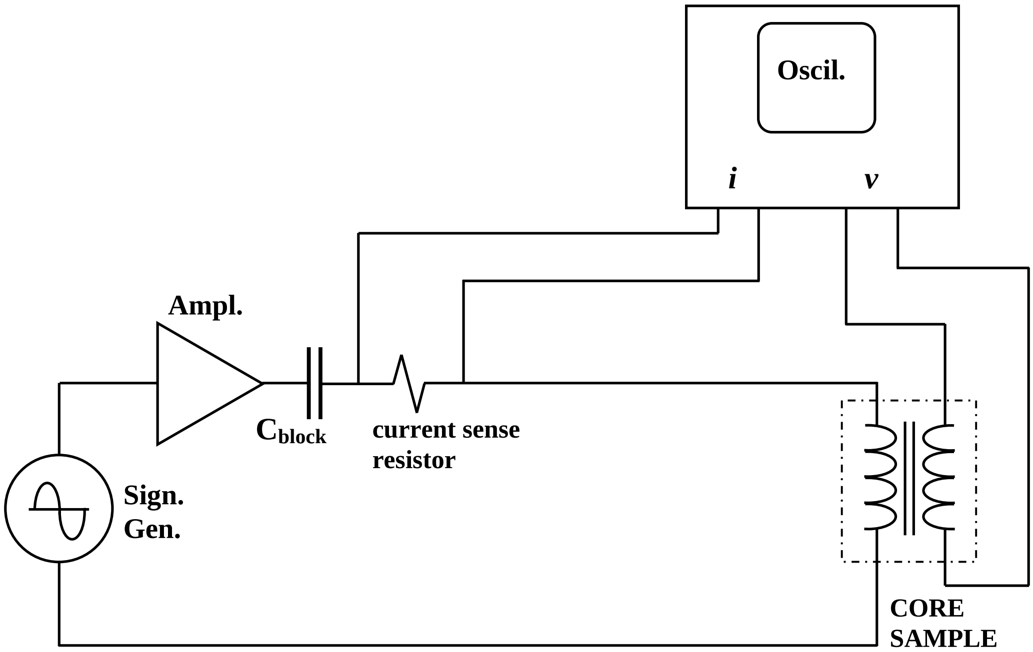

Fig. 3.2 : Normal curve measurement circuit.

The shunt resistor was 1 Ω ±1 % x 10 W metal film, with a parasite inductance of 4.1 μH.

To check the normal curve agreement with the static curve one may verify that the measured inductance does not vary with the frequency.

This was done for material 3C85 with $B_m = 0.2$ T. Results are presented in Table 3.1.

TABLE 3.1:Measurements with material 3C85

f [Hz]	$V_{P\,rms}$ [mV]	I_{rms} [mA]	I_{P-P} [mA]	L [mH]
50	115.45	44.20	127.0	8.3135
100	230.90	44.33	129.0	8.2891
250	577.20	44.73	131.7	8.2150
500	1154.4	44.95	132.3	8.1748
1000	2308.8	44.88	132.3	8.1875
2000	4617.6	44.82	132.0	8.1985
4000	9235.2	44.80	131.8	8.2021
10000	23090.0	44.98	132.4	8.1693
20000	46176.0	44.65	131.1	8.2297

A frequency of 1000Hz was adopted to obtain the normal curves because it is a frequency low enough but the voltages needed at lower inductions are sufficiently high to be measured without problems.

As the curves were obtained using 50 turns windings, the dc current to be injected with other number of turns (n_x) is given by: $I_{dc} = \dfrac{50}{n_x}\dfrac{I_{P-P}}{2}$.

III - 2.2 *Twin cores measurement method*

Using two equal set of cores it is possible to duplicate the active power to be measured while keeping separated core volume small enough to facilitate power dissipation. Thus, the internal material temperature is more uniform and also the thermal constant are lower, allowing shorter cooling intervals between measurements. Moreover, it is possible to use isolated dc bias windings connected with opposite phase, in order to prevent power dissipation into the dc bias circuit.

The schematic circuit is presented in Fig. 3.3 . Notice, that the blocking capacitor is not longer required (provided that both the signal generator and the power amplifier do not introduce offset).

In order to obtain accurate results, both cores should have well matched material characteristics.

Averaging the normal curves determined for each core, one obtains the equivalent static curve to be used for biasing purposes.

For example, the normal curve dispersion found for material 3F3 was 10 %, this yields ± 5 % dispersion regarding the average curve.

This lack of accuracy regarding the dc bias , may be a drawback when aiming to characterize a particular material sample behavior, but it would be not important if the average typical material characteristics are searched.

Looking for equal alternative induction, primary windings are connected in parallel, while secondary sense voltage windings are serially connected to get the average sense voltage.

To ensure that the alternative power, dissipated into the dc bias circuit, be negligible, the ac blocking inductor is retained.

As the accuracy achieved in power measurements with the available instruments was 9 % , an accuracy of 5 % in dc bias induction was considered acceptable. Therefore, this method was selected to do the experimental measurements.

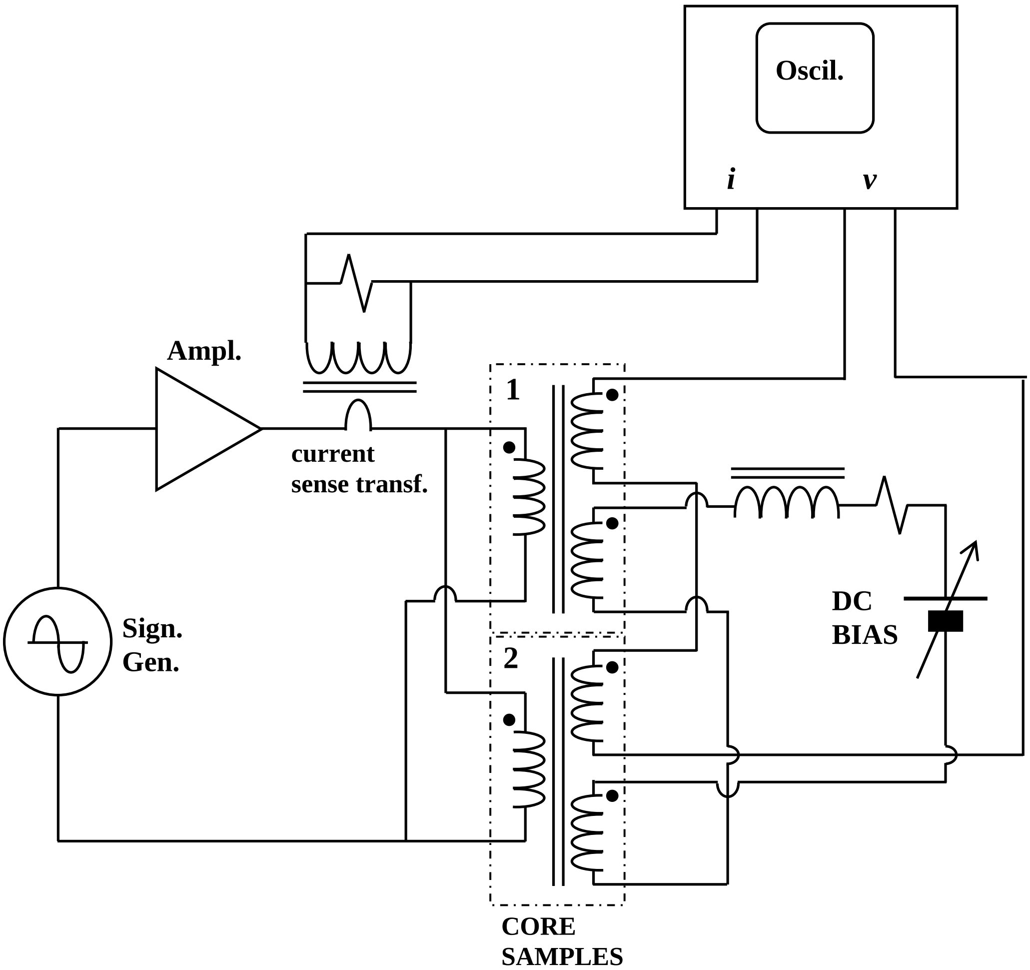

Fig. 3.3 : Twin cores measurement circuit.

III - 3. MEASUREMENTS IMPROVING THE APPARENT POWER FACTOR

In order to overcome the poor accuracy due to the low power factor (explained in section III-1.3), a loss-less capacitor might be connected in parallel with primary windings.

Vacuum, air or glass capacitors do not have enough capacity for this application and, unfortunately, the losses introduced by other capacitors would wreck the possible accuracy gain.

For example, a polystyrene film capacitor exhibits a power factor of 0.0033 @ 35 Vrms, 25 kHz. Thus the introduced losses become as important as the power loss to be measured.

To overcome this problem, the power factor measured will be improved rather the actual one. That is, an apparent power factor will be improved.

To do this, the current signal will be derived by means of a loss-less Rogowski transformer [4] and the resulting signal (properly scaled) will be subtracted from the voltage signal. By this way, the voltage component in quadrature with the current signal will be reduced and the measured apparent power factor will be improved.

As only the active power will be measured, the amplitude accuracy of the derived current signal is not important. Only an accurate and stable $\pi/2$ phase shift is mandatory to achieve good accuracy.

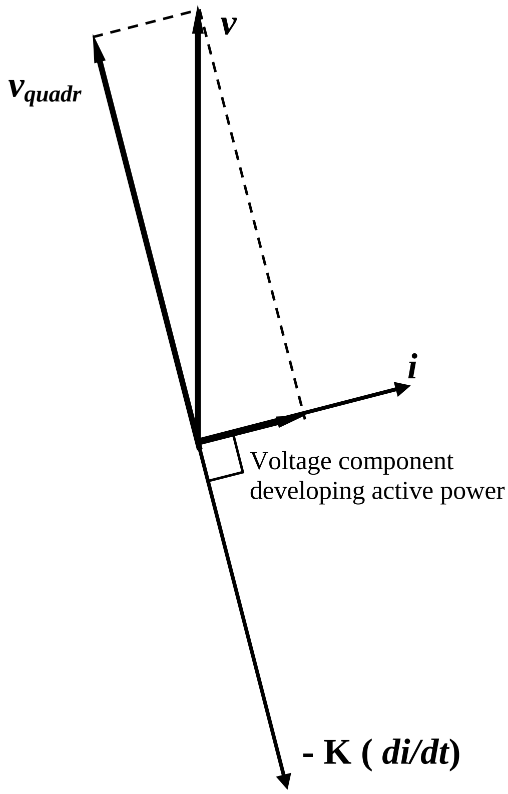

Fig. 3.4 : Principles of measurement improving the apparent power factor.

Approaching saturation the current becomes distorted but the method will not introduce errors, because the derivative of each harmonic component of the current is phase shifted $\pi/2$, and does not contribute to the measured power, even if the voltage signal has multiple harmonic components.

When the current becomes distorted by the core saturation, the voltage signal is also distorted in the same way, due to the series impedance, which is linear because it is formed by the leakage inductance (with air flux path) plus the series resistance of primary windings. Therefore, the measured power without power factor compensation will be:

$$P_1 = \frac{1}{T}\int_0^T \left(\sum_{k=1}^{\infty} v_k \sum_{k=1}^{\infty} i_k \right) dt = \sum_{k=1}^{\infty} P_k$$

Introducing the power factor compensation the measured power will be:

$$P_2 = \frac{1}{T}\int_0^T \left(\sum_{k=1}^{\infty} v_k - K\frac{d}{dt}\sum_{k=1}^{\infty} i_k \right) \sum_{k=1}^{\infty} i_k \; dt = \frac{1}{T}\int_0^T \left(\sum_{k=1}^{\infty} v_k \sum_{k=1}^{\infty} i_k \right) dt - \frac{K}{T}\int_0^T \left(\sum_{k=1}^{\infty} i_k \sum_{k=1}^{\infty} \frac{d\, i_k}{dt} \right) dt$$

but, $\frac{K}{T}\int_0^T \left(\sum_{k=1}^{\infty} i_k \sum_{k=1}^{\infty} \frac{d\, i_k}{dt} \right) dt = 0$ (because all the harmonic components involved in the products are orthogonal functions) so, finally results $P_2 = P_1$. Thus, the power factor compensation does not alter the measured power. Moreover, this might allow using this measurement improvement technique with non sinusoidal waveforms.

The most promising feature of this method is that it might allow testing components having large air gaps.

In order to test the derivative performance, one Rogowski transformer was assembled winding two Rogowski coils on the same toroidal air core. The derived current signal matched quite well the digital derivative done by the digital oscilloscope.

The use of a Rogowski transformer instead of a single Rogowski coil allows overcoming the poor sensitivity of the single coil for small currents. Moreover, the flux is better confined inside the toroid giving both a more stable signal and higher noise immunity.

Further exploration of this proposed technique will be done in future works.

III - 4. CONCLUSIONS AND FUTURE WORK

1. From the experimental measurements done, one may conclude that for the particular case of flyback converters operating in discontinuous mode at low frequency (i.e. 25 kHz) and designed for minimum core volume, the classical Steinmetz equation may be applied for transformer design. This is possible because in such cases the design is limited by saturation and also, the dc bias is usually lower than half of the maximum induction attained.

   In such conditions the core losses are smaller or hardly bigger than the ones corresponding to the unbiased condition. Moreover, as the duty factor is usually adopted near 50 % , the non sinusoidal waveform does not significatively affect losses so, using ESE or iGSE might not be necessary.

2. If a flyback transformer has to be optimized from the efficiency point of view (minimizing losses) the optimal maximum induction should be reduced [5]. In this case, the dc bias may increase the losses with respect to the classical Steinmetz results.

3. If an asymmetrical converter has to operate at high frequency, the maximum allowable induction is limited by losses at values that exhibit great variations depending upon the bias adopted. In this case the dc bias will have a strong influence in transformer design. This will be true in the particular case of quasi-resonant converters, where the switching frequency adopted is the highest possible, but the goal is to reach very high efficiencies.

4. In order to test the loss prediction models many samples from different materials need to be characterized varying frequency, maximum alternative induction, dc bias and eventually temperature. This requires such a large number of measurements that some form of automatic instrument should be developed.

   A B-H analyzer capable of measuring losses using the most common waveforms in power electronics might be developed as a student project. The default waveform operation should be sinewave and the power factor compensation should be included as selectable function.

5. The dc bias and non-sinusoidal waveform influence may be considered using different approaches based upon sinewave made measurements. This suggest that a convenient way for the manufacturers to specify their products is to give the family of curves plotted with sinusoidal drive under dc bias conditions. To obtain these families of curves many samples of each material should be measured in order to get the average results.

   Again, this would be only feasible having an automatic measurement system.

6. As future work, the joint application of the models dealing with both minor loops and dc bias will be used to calculate the core losses in power factor corrector circuits.

APPENDIX B
EFFECTIVE PERMEABILITY ESTIMATION

The effective permeability may be expressed as function of an equivalent air gap section S_a , defined assuming that: $\Phi = B_a\ S_a = B_{Fe}\ S_{Fe}$. With this assumption, the effective permeability becomes:

$$\mu_{r_e} = \frac{\mu_r}{1+\mu_r\ \frac{l_a}{l_{Fe}}\left(\frac{S_{Fe}}{S_a}\right)} = \frac{1}{\frac{1}{\mu_r}+\frac{l_a}{l_{Fe}}\left(\frac{S_{Fe}}{S_a}\right)} \qquad \text{(B.1).}$$

From Fig. B.1, this air gap section is roughly approximated considering that the magnetic path section inside the core is enlarged due to the fringing effect, in a length proportional to the air gap width. With this assumption, the equivalent air gap section is proposed in Fig. B.2.

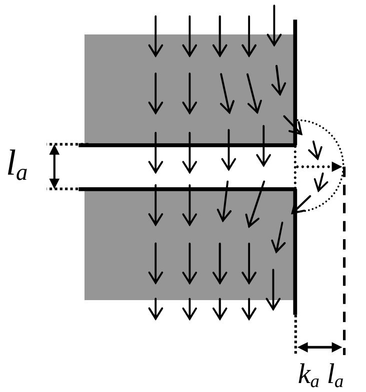

Fig. B.1 : Fringing effects

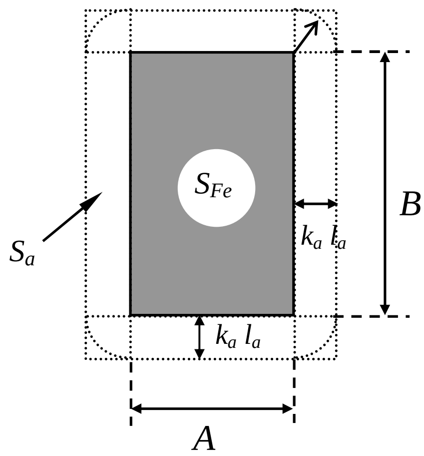

Fig. B.2 : Air gap equivalent section

Based upon the approach of Fig. B.2, the air gap equivalent section is given by:

$$\frac{S_a}{S_{Fe}} = 1+2\left(1+\frac{A}{B}\right)\left(\frac{k_a\ l_a}{A}\right)+\pi\left(\frac{A}{B}\right)\left(\frac{k_a\ l_a}{A}\right)^2 \qquad \text{(B.2).}$$

This result should be utilized in eq. B.1 to obtain the effective permeability, and next the A_L factor may be obtained as:

$$A_L = \frac{0.4\ \pi\ \mu_{re}}{\Sigma\left(l/A\right)}\ [nH] \qquad \text{(B.3).}$$

The value of k_a may range from 0.7 to 1.9 , and for a central leg air gap may be approximated by [6]:

$$k_a = 0.241+\frac{1}{\pi}\ln\frac{b_w}{l_a} \qquad \text{(B.4)}$$

where b_w is the winding window width.

When the air gap is shared between the external and central legs, experimental measures show that the approximative formula may be still used, because the air gap width reduction is partially compensated by an increment of k_a .

REFERENCES

[1] S.-C Wang and C.-L. Chen, "PC-based apparatus for characterising high frequency magnetic cores", *IEE Proc. - Sci. Meas. Technology* , Vol. 146, no. 6, U.K., Nov. 1999.

[2] R. Linkous, A. W. Kelley, and K. C. Armstrong, "An improved calorimeter for measuring the core loss of magnetic materials", *Applied Power Electronics Conf. and Expo. 2000 (IEEE - APEC 2000).*

[3] G. Bertotti, "Hysteresis in magnetism", Academic Press, 1998, (Chap. 1 - Sect. 1.2).

[4] G. D'Antona et al., "AC measurements via digital processing of Rogowski coils signal", *IEEE Instrumentation and Measurement Technology Conference* , Anchorage, USA, May 2002.

[5] H.E. Tacca, "Flyback vs. Forward Converter Topology Comparison Based upon Magnetic Design", *Eletrônica de Potência* , Vol. 5, no. 1, May 2000, Brazil.

[6] E. C. Snelling, "Soft Ferrites: Properties and Applications", Butterworths, U.K., 1988 (Chap. 4 - Sect. 4.2.2).

APPENDIX C

EXPERIMENTAL RESULTS

NORMAL CURVE

Material: **3C85** Ferroxcube

Frequency: **1 kHz**

B_m [T]	*VOLTAGE* [Vrms]	(50 turns) I_{rms} [mA]	(50 turns) I_{p-p} [mA]	(5 turns) I_{dc} [mA]
0.025	0.2886	5.78	15.66	78.30
0.05	0.5772	11.70	33.24	166.20
0.1	1.1544	22.40	64.10	320.50
0.15	1.7316	33.50	97.00	485.00
0.2	2.3088	44.84	132.30	661.50
0.25	2.8860		58.10 175.20	876.00
0.3	3.4632		75.00 240.00	1200.00

B_{ac} [T] / **B_{dc} [T]**	**0.025**	**0.05**	**0.1**	**0.15**	**0.2**	**0.25**	**0.3**
0.0	1.260 1.350 1.340	6.770 6.900 7.000	35.900 35.700 36.100	99.500 100.000 101.500	200.000 203.600 209.000	344.000 342.000	527.000 525.000 518.000
0.025	1.210 1.200	6.710 6.690	35.900 36.300	99.000 100.700	203.000 205.000	342.000 344.000	524.000 521.000
0.05	1.180 1.250	6.600 6.590	36.800 36.500	100.000 102.000	203.800 207.000	339.600 337.500 341.000	**SAT**
0.1	1.360 1.314	7.820 7.840	41.700 42.100	106.400 107.000 111.000	216.000 217.500	345.000 347.000 348.500	
0.15	1.640 1.620	10.340 9.700	52.500 51.900	120.200 120.700 123.000	224.000 229.000	**SAT**	
0.2	2.570 2.500	14.100 13.380	66.500 66.100	130.600 130.850	**SAT**		
0.25	3.900 3.780	19.780 20.050 19.560	80.300 80.200	**SAT**			
0.3	7.220 7.120	30.100 29.530	**SAT**				

CORE LOSS [mW]
CORE: **E/25/13/7**

MATERIAL: **3C85** Ferroxcube

FREQUENCY: **25 kHz**

AC WINDINGS: **5 turns**

B_{ac} [T] / B_{dc} [T]	**0.025**	**0.05**	**0.1**	**0.15**	**0.2**	**0.25**	**0.3**
0.0	2.150 2.180	14.590 14.290 14.440	78.100 77.150	228.500 228.750	476.620 474.300 477.000	826.620 823.620	1277.000 1275.620
0.025	2.050 1.980	14.250 14.300	76.650 76.990	227.750 227.350	474.250 471.330	818.870 824.500	1271.000 1272.870
0.05	2.040 1.940	14.520 14.420	77.910 78.680	227.870 228.370	475.000 475.620	821.620 819.620	1267.250 1265.120
0.1	2.250 2.150	16.790 16.730	88.920 89.210	247.000 246.120	498.870 499.120	838.000 842.870 846.370 841.250	1277.620 1276.620 1275.870
0.15	2.500 2.460	21.020 20.770	109.110 108.350	278.870 279.620	534.120 533.750	870.370 867.250	**SAT**
0.2	3.750 3.720	27.080 26.810	133.000 132.000	315.750 312.750		**SAT**	
0.25	6.050 5.950	36.300 35.900	159.620 159.750	**SAT**			
0.3	10.200 10.100	47.190 47.120	**SAT**				

CORE LOSS [mW]
CORE: **E/25/13/7**
MATERIAL: **3C85** Ferroxcube
FREQUENCY: **50 kHz**
AC WINDINGS: **5 turns**

B_{ac} [T] / B_{dc} [T]	**0.025**	**0.05**	**0.1**	**0.15**	**0.2**	**0.25**	**0.3**
0.0	5.490 6.060 5.340 5.980	38.290 36.620 35.800 35.550	222.120 220.620 220.870	606.620 609.750 608.750 611.370	1277.620 1297.250 1289.000	2230.870 2245.500 2238.500	3480.000 3451.250 3462.500
0.025	5.580 5.590 5.660	36.250 36.150 36.110	219.250 220.500 220.000	610.250 604.750 605.120	1288.870 1282.870 1291.750	2230.250 2228.120 2232.290	**T ≠ Cnt**
0.05	5.640 5.520 5.590	36.640 36.220 36.210	222.370 222.500 221.370	607.620 614.250 614.250	1294.370 1288.870 1286.000	2229.370 2232.750 2238.500	**T ≠ Cnt**
0.1	6.000 5.850 5.820	41.670 41.290 40.900	248.250 248.120 249.000	661.500 659.870 656.000	1345.750 1341.250 1339.000	2273.370 2261.750 2270.870	**SAT**
0.15	7.740 7.410 7.390	52.500 52.450 52.290	286.120 286.120 284.120	739.000 739.120 737.750	1414.620 1418.370 1417.250	2313.750 2307.500	
0.2	9.560 9.700 9.740	68.190 68.430 68.020	348.620 347.370 347.120	818.500 817.370 817.500	1474.500 1474.100	**SAT**	
0.25	15.460 15.770 15.710	94.350 94.290 94.020	411.120 412.620 411.370	893.620 892.620 896.370	**SAT**		
0.3	28.240 28.010 28.050	101.840 102.720 102.620	486.750 486.870 484.870	**SAT**			

CORE LOSS [mW]
CORE: **E/25/13/7**

MATERIAL: **3C85** Ferroxcube

FREQUENCY: **100 kHz**

AC WINDINGS: **5 turns**

B_{ac} [T] / B_{dc} [T]	0.025	0.05	0.1	0.15 (5 turns)	0.2 (2 turns)	0.25	0.3
0.0	19.590 19.520 19.550	120.910 120.310 119.760	668.000 666.620 668.000	1871.000 1874.750 1875.000	4056.250 4083.750 4022.500 4108.750		
0.025	19.620 19.420 19.400	118.200 118.040 117.620	666.620 664.750 666.250	1870.750 1868.870 1871.120	4026.250 4037.500 3950.000		
0.05	20.170 20.000 20.040	119.610 118.650 119.950	664.000 661.000 660.500	1880.500 1884.870 1883.750	3995.000 3997.500 4023.700		
0.1	22.670 22.270 22.220	133.690 132.270 131.610	725.500 725.620 725.370	2002.870 2003.250 1997.370	4025.000 4133.700 4165.000		
0.15	26.070 26.000 26.160	165.200 164.120 163.390	874.500 872.370 872.250	2222.370 2213.750 2217.250	4177.500 4223.700 4267.500		
0.2	31.750 31.470 31.950	212.750 211.750 210.750	1044.620 1044.850 1045.500	2443.120 2464.370 2427.120	4371.250 4372.500 4413.750		
0.25	45.860 47.370 47.100	276.750 276.120 276.500	1185.880 1197.500 1202.500	**SAT**	**SAT**		
0.3	75.640 74.500 74.000	338.620 330.370 326.630	1273.000 1272.250				

CORE LOSS [mW]
CORE: **E/25/13/7**

MATERIAL: **3C85** Ferroxcube

FREQUENCY: **200 kHz**

AC WINDINGS: **5 and 2 turns**

B_{ac} [T] / B_{dc} [T]	0.025	0.05	0.1	0.15	0.2	0.25	0.3
0.0	53.090 52.970 53.090	266.870 264.880 264.500	1439.750 1431.250 1433.120	3922.500 3917.500 3946.250			
0.025	53.640 53.370 53.170	261.250 259.750 258.750	1427.000 1422.500 1418.870	**T ≠ Cnt**			
0.05	55.150 54.870 54.760	258.000 257.120 257.000	1416.120 1418.620 1417.750				
0.1	57.840 57.450 57.310	272.120 271.870 271.000	1471.370 1468.370 1462.000				
0.15	62.590 61.790 61.540	307.750 306.620 305.370	1625.120 1628.370 1630.370				
0.2	70.410 69.850 69.450	365.000 365.370 363.870	1887.870 1881.370 1878.370				
0.25	79.440 78.860 78.720	463.870 464.000 461.500	2180.620 2173.000 2170.870				
0.3	118.990 119.420 119.080	631.000 634.870 638.620	**SAT**				

CORE LOSS [mW]
CORE: **E/25/13/7**

MATERIAL: **3C85** Ferroxcube

FREQUENCY: **300 kHz**

AC WINDINGS: **2 turns**

NORMAL CURVE

Material: 3F3 Ferroxcube

Frequency: 1 kHz **(DC induction bias error < ± 5 %)**

B_m [T]	VOLTAGE [Vrms]	I_{p-p} (50 turns) [mA]		(5 turns) I_{dc} [mA]
		core # 1	core # 2	
0.025	0.2886		21.06 19.50	101
0.05	0.5772	41.43	38.16	199
0.1	1.1544	80.60	73.32	385
0.15	1.7316	119.60	110.90	576
0.2	2.3088	161.10	148.40	774
0.25	2.8860	206.00	191.40	994
0.3	3.4632	263.80	246.40	1276

B_{ac} [T] / B_{dc} [T]	**0.025**	**0.05**	**0.1**	**0.15**	**0.2**	**0.25**	**0.3**
0.0	1.275 1.305 1.317	5.637 5.725 5.650	30.987 31.012 30.800	89.437 88.050 89.037	188.750 187.375 188.125	345.000 344.750 344.250	550.25 550.500 553.875
0.025	1.265 1.229 1.272	5.525 5.575 5.475	30.587 30.700 30.587	88.312 87.176 87.875	186.750 186.250 187.500	339.500 340.750 340.000	545.375 544.875 546.625
0.05	1.261 1.210 1.240	5.475 5.500 5.450	30.531 30.575 30.375	87.250 86.675 87.662	187.000 185.750 186.625	336.250 336.750 338.000	536.000 536.125 537.875
0.1	1.300 1.266 1.312	5.675 5.725 5.637	32.075 32.200 31.962	92.000 91.000 91.500	193.875 193.125 194.125	346.500 343.875 344.500	543.625 535.875 537.750
0.15	1.420 1.367 1.396	6.537 7.050 6.537	36.487 36.537 36.387	102.000 101.375 102.375	209.500 209.000 210.250	366.000 366.620 370.870	**SAT**
0.2	1.656 1.616 1.662	7.975 7.975 7.987	43.037 42.712 42.700	117.250 116.000 117.000	233.125 233.000 235.125	**SAT**	
0.25	2.094 2.047 2.090	10.175 10.112 10.162	52.787 52.687 52.650	140.250 138.375 139.250	**SAT**		
0.3	3.261 3.284 3.307	14.550 14.537 14.650	73.787 74.762 70.200	**SAT**			

CORE LOSS [mW]
CORE: **E/25/13/7**

MATERIAL: **3F3** Ferroxcube

FREQUENCY: **25 kHz**

AC WINDINGS: **5 turns**

B_{ac} [T] / B_{dc} [T]	**0.025**	**0.05**	**0.1**	**0.15**	**0.2**	**0.25**	**0.3**
0.0	2.311 2.215 2.311	12.325 11.988 12.125	64.275 64.480 63.487	188.500 185.375 186.375	421.250 417.375 418.750	761.875 753.750 759.375	1177.370 1158.120 1164.120
0.025	2.188 2.088 2.327	11.925 11.738 11.525	63.737 64.637 62.887	185.875 184.875 187.625	415.000 413.000 416.500	750.375 743.875 757.875	**T ≠ Cnt**
0.05	2.623 2.952 2.904	11.412 11.687 11.500	65.262 63.375 62.400	186.500 184.000 185.750	412.125 410.375 412.500	749.500 743.750 750.250	**T ≠ Cnt**
0.1	2.994 3.105 3.205	12.062 12.150 11.875	64.500 65.360 64.975	196.375 194.375 197.375	424.750 424.000 428.625	760.625 760.625 771.625	**SAT**
0.15	3.398 3.237 2.960	13.587 13.775 13.675	76.250 75.375 73.625	219.750 217.125 219.625	452.375 448.875 452.750	793.750 782.625 787.750	
0.2	3.187 3.325 3.475	16.800 16.862 16.650	88.500 89.750 89.750	243.875 242.250 246.125	482.750 488.125 484.500	**SAT**	
0.25	5.025 5.062 5.025	22.225 22.162 22.475	107.250 108.000 105.125	**SAT**	**SAT**		
0.3	6.637 6.250 6.062	27.862 27.737 28.625	**SAT**				

CORE LOSS [mW]
CORE: **E/25/13/7**

MATERIAL: **3F3** Ferroxcube

FREQUENCY: **50 kHz**

AC WINDINGS: **5 turns**

B_{ac} [T] / B_{dc} [T]	**0.025**	**0.05**	**0.1**	**0.15**	**0.2**	**0.25**	**0.3**
0.0	3.775 3.750 3.637 3.712	22.925 22.037 22.150 22.200	130.125 129.375 129.625	431.500 431.000 432.625	1074.500 1072.500 1071.375	2203.700 2240.000 2266.200	3611.250 3595.000 3610.000
0.025	3.400 3.325 3.212	21.725 21.500 21.225	128.125 127.875 128.875	426.125 426.625 427.500	1044.750 1054.000 1057.750	2181.250 2150.000 2240.200	**T ≠ Cnt**
0.05	3.125 3.225 3.262	21.262 21.412 21.500	129.875 128.875 128.500	426.750 429.000 427.875	1033.500 1032.375 1032.620	2235.000 2197.500 2235.000	**T ≠ Cnt**
0.1	3.600 3.487 3.350	23.237 23.025 22.775	141.625 142.000 143.125	468.250 463.875 465.250	1067.750 1062.750 1074.120	2230.000 2255.000 2248.700	**SAT**
0.15	3.837 3.912 3.950	27.400 27.462 27.500	175.125 174.375 174.625	572.750 563.750 560.000 540.750	1214.370 1200.870 1234.620	**SAT**	
0.2	4.812 4.712 4.550	34.575 34.025 33.537	217.875 219.750 221.125	635.500 644.500 641.620	**SAT**		
0.25	6.375 6.487 6.575	43.837 44.062 44.087	266.125 264.875 264.500	738.500 739.000 741.000			
0.3	10.025 9.887 9.675	52.462 51.987 51.287	311.875 313.875 315.500	**SAT**			

CORE LOSS [mW]
CORE: **E/25/13/7**

MATERIAL: **3F3** Ferroxcube

FREQUENCY: **100 kHz**

AC WINDINGS: **5 turns**

B_{ac} [T] / B_{dc} [T]	0.025	0.05	0.1	0.15	0.2	0.25	0.3
0.0	13.812 13.712 13.675	65.637 67.100 66.300	440.125 438.500 442.875	1378.375 1372.375 1384.750	3386.250 3557.500 3485.000	**T ≠ Cnt**	
0.025	13.100 13.137 13.237	63.100 63.162 62.400	441.250 435.875 436.000	1368.250 1353.125 1346.750	3540.000 3578.750 3487.500		
0.05	13.637 13.537 13.450	62.650 62.910 63.012	440.000 441.000 444.375	1385.750 1384.750 1379.250	3475.500 3521.250 3586.250		
0.1	14.462 14.450 14.512	66.725 66.212 65.625	479.750 476.875 475.875	1469.250 1463.250 1473.500	3680.000 3651.250 3676.250		
0.15	14.600 14.712 14.637	72.875 73.250 73.375	547.125 551.125 555.000	1670.125 1667.250 1675.000	4122.500 4156.250 4253.750		
0.2	15.962 16.012 15.762	85.875 85.250 84.250	656.125 656.875 660.750	1992.500 1920.000 1978.750	**SAT**		
0.25	18.575 18.275 18.125	105.000 105.375 105.500	804.500 802.000 800.500	**SAT**			
0.3	20.450 20.425 20.525	147.375 146.875 145.625	**SAT**				

CORE LOSS [mW]
CORE: **E/25/13/7**

MATERIAL: **3F3** Ferroxcube

FREQUENCY: **200 kHz**

AC WINDINGS: **2 turns**

B_{ac} [T] / B_{dc} [T]	0.025	0.05	0.1	0.15	0.2	0.25	0.3
0.0	24.850 24.750 24.550	77.450 77.400 77.625	331.750 331.375 330.750	929.000 933.250 925.375			
0.025	24.212 24.312 24.325	76.212 76.212 75.612	328.375 328.000 328.000	920.000 914.625 919.750			
0.05	24.500 24.362 24.200	74.400 73.962 74.087	328.375 327.000 327.000	926.500 926.125 925.750			
0.1	25.312 25.375 25.350	75.075 74.712 75.200	336.000 335.750 336.375	933.500 946.125 944.125			
0.15	26.550 26.350 26.037	78.075 77.475 77.100	360.375 358.000 357.750	1053.500 1063.375 1071.750			
0.2	28.412 28.562 28.537	82.550 82.500 82.725	392.125 393.250 394.500	**Ampl. limit**			
0.25	29.837 29.650 29.350	88.900 88.750 88.087	466.875 464.625 464.125				
0.3	32.250 32.387 32.350	93.825 94.150 94.112	**SAT**				

CORE LOSS [mW]
CORE: **E/25/13/7**

MATERIAL: **3F3** Ferroxcube

FREQUENCY: **400 kHz**

AC WINDINGS: **2 turns**

AVERAGE RESULTS

<u>UNITS:</u> **Core Losses in mW** **Magnetic Induction in T**

CORE: E25/13/7 **MATERIAL: 3C85** **FREQUENCY: 25 kHz**

B_{dc} \ B_{ac}	**0.025**	**0.05**	**0.1**	**0.15**	**0.2**	**0.25**	**0.3**
0.0	1.317	6.890	35.900	100.333	204.200	343.000	523.333
0.025	1.205	6.700	36.100	99.850	204.000	343.000	522.500
0.05	1.215	6.595	36.650	101.000	205.400	339.367	518.000
0.1	1.337	7.830	41.900	108.133	216.750	346.833	
0.15	1.630	10.020	52.200	121.300	226.500		
0.2	2.535	13.740	66.300	130.725			
0.25	3.840	19.797	80.250				
0.3	7.170	29.815					

CORE: E25/13/7 **MATERIAL: 3C85** **FREQUENCY: 50 kHz**

B_{dc} \ B_{ac}	**0.025**	**0.05**	**0.1**	**0.15**	**0.2**	**0.25**	**0.3**
0.0	2.165	14.440	77.625	228.625	475.973	825.120	1276.310
0.025	2.015	14.275	76.820	227.550	472.790	821.685	1271.935
0.05	1.990	14.470	78.295	228.120	475.310	820.620	1266.185
0.1	2.200	16.760	89.065	246.560	498.995	842.122	1276.703
0.15	2.480	20.895	108.730	279.245	533.935	868.810	
0.2	3.735	26.945	132.500	314.250			
0.25	6.000	36.100	159.685				
0.3	10.150	47.155					

CORE: E25/13/7 **MATERIAL: 3C85** **FREQUENCY: 100 kHz**

B_{dc} \ B_{ac}	**0.025**	**0.05**	**0.1**	**0.15**	**0.2**	**0.25**	**0.3**
0.0	5.717	36.565	221.203	609.122	1287.957	2238.290	3464.583
0.025	5.610	36.170	219.917	606.707	1287.830	2230.220	
0.05	5.583	36.357	222.080	612.040	1289.747	2233.540	
0.1	5.890	41.287	248.457	659.123	1342.000	2268.663	
0.15	7.513	52.413	285.453	738.623	1416.747	2310.625	
0.2	9.667	68.213	347.703	817.790	1474.300		
0.25	15.647	94.220	411.703	894.203			
0.3	28.010	102.393	486.163				

AVERAGE RESULTS

UNITS: **Core Losses in mW** **Magnetic Induction in T**

CORE: E25/13/7	**MATERIAL: 3C85**	**FREQUENCY: 200 kHz**					
B_{ac} / B_{dc}	**0.025**	**0.05**	**0.1**	**0.15**	**0.2**	**0.25**	**0.3**
0.0	19.553	120.327	667.540	1873.583	4067.812		
0.025	19.480	117.953	665.873	1870.247	4004.583		
0.05	20.070	119.403	661.833	1883.040	4005.400		
0.1	22.387	132.523	725.497	2001.163	4107.900		
0.15	26.077	164.237	873.040	2217.790	4222.900		
0.2	31.723	211.750	1044.990	2444.870	4385.833		
0.25	46.777	276.457	1195.293				
0.3	74.713	331.873	1272.625				

CORE: E25/13/7	**MATERIAL: 3C85**	**FREQUENCY: 300 kHz**					
B_{ac} / B_{dc}	**0.025**	**0.05**	**0.1**	**0.15**	**0.2**	**0.25**	**0.3**
0.0	53.050	265.417	1434.707	3928.750			
0.025	53.390	259.917	1422.790				
0.05	54.927	257.373	1417.497				
0.1	57.533	271.663	1467.247				
0.15	61.973	306.580	1627.953				
0.2	69.903	364.747	1882.537				
0.25	79.007	463.120	2174.830				
0.3	119.163	634.830					

AVERAGE RESULTS

UNITS: **Core Losses in mW** **Magnetic Induction in T**

CORE: E25/13/7 **MATERIAL: 3F3** **FREQUENCY: 25 kHz**

B_{dc} \ B_{ac}	0.025	0.05	0.1	0.15	0.2	0.25	0.3
0.0	1.299	5.671	30.933	88.841	188.083	344.667	551.542
0.025	1.255	5.525	30.625	87.788	186.833	340.083	545.625
0.05	1.237	5.475	30.494	87.196	186.458	337.000	536.667
0.1	1.293	5.679	32.079	91.500	193.708	344.958	539.083
0.15	1.394	6.708	36.470	101.917	209.583	367.830	
0.2	1.645	7.979	42.816	116.750	234.083		
0.25	2.077	10.150	52.708	139.292			
0.3	3.284	14.579	72.916				

CORE: E25/13/7 **MATERIAL: 3F3** **FREQUENCY: 50 kHz**

B_{dc} \ B_{ac}	0.025	0.05	0.1	0.15	0.2	0.25	0.3
0.0	2.279	12.146	64.081	186.750	419.125	758.333	1166.537
0.025	2.201	11.729	63.754	186.125	414.833	750.708	
0.05	2.826	11.558	63.679	185.417	411.667	747.833	
0.1	3.101	12.029	64.945	196.042	425.792	764.292	
0.15	3.198	13.679	75.083	218.833	451.333	788.042	
0.2	3.329	16.771	89.333	244.083	485.125		
0.25	5.037	22.287	106.792				
0.3	6.316	28.075					

CORE: E25/13/7 **MATERIAL: 3F3** **FREQUENCY: 100 kHz**

B_{dc} \ B_{ac}	0.025	0.05	0.1	0.15	0.2	0.25	0.3
0.0	3.718	22.328	129.708	431.708	1072.792	2236.633	3605.417
0.025	3.312	21.483	128.292	426.750	1052.167	2190.483	
0.05	3.204	21.391	129.417	427.875	1032.832	2222.500	
0.1	3.479	23.012	142.250	465.792	1068.207	2244.567	
0.15	3.900	27.454	174.708	559.312	1216.620		
0.2	4.691	34.046	219.583	640.54			
0.25	6.479	43.995	265.167	739.500			
0.3	9.862	51.912	313.750				

AVERAGE RESULTS

UNITS: **Core Losses in mW** **Magnetic Induction in T**

CORE: E25/13/7	**MATERIAL: 3F3**	**FREQUENCY: 200 kHz**

B_{dc} \ B_{ac}	**0.025**	**0.05**	**0.1**	**0.15**	**0.2**	**0.25**	**0.3**
0.0	13.733	66.346	440.500	1378.500	3476.250		
0.025	13.158	62.887	437.708	1356.042	3535.417		
0.05	13.541	62.857	441.792	1383.250	3527.667		
0.1	14.475	66.187	477.500	1468.667	3669.167		
0.15	14.650	73.167	551.083	1670.792	4177.500		
0.2	15.912	85.125	657.917	1963.750			
0.25	18.325	105.292	802.333				
0.3	20.467	146.625					

CORE: E25/13/7	**MATERIAL: 3F3**	**FREQUENCY: 400 kHz**

B_{dc} \ B_{ac}	**0.015**	**0.025**	**0.05**	**0.075**	**0.1**	**0.15**	**0.2**
0.0	24.717	77.492	331.292	929.208			
0.025	24.283	76.012	328.125	918.125			
0.05	24.354	74.150	327.458	926.125			
0.1	25.346	74.996	336.042	941.250			
0.15	26.312	77.550	358.708	1062.875			
0.2	28.504	82.592	393.292				
0.25	29.612	88.579	465.208				
0.3	32.329	94.029					

BIBLIOGRAPHY

1. E. Della Torre, “Magnetic Hysteresis”, IEEE Press and J. Wiley, 1999.
2. G. Bertotti, “Hysteresis in Magnetism”, Academic Press, 1998.
3. E. C. Snelling, “Soft Ferrites: Properties and Applications”, Butterworths, U.K.,1988.
4. R. F. Soohoo, “Theory and Applications of Ferrites”, Prentice-Hall, 1960.
5. S. Smith, “Magnetic Components: Design and Applications”, Van Nostrand Reinhold, 1985.
6. A. Goldman, “Magnetic Components for Power Electronics”, Kluwer Academic Publ., 2002.
7. R. Boll (editor), “Soft magnetics materials: fundamentals, alloys, properties, products and applications”, Heyden, U.K., 1978.
8. C. W. McLyman, “Magnetic Core Selection for Transformers and Inductors”, M. Dekker, 1997.
9. W. M. Flanagan, “Handbook of Transformer Design and Applications”, McGraw-Hill, 1992.
10. R. M. Bozorth, “Ferromagnetism”, IEEE Press, 1994.
11. M.I.T., E.Eng. Staff, “Magnetic Circuits and Transformers”, The MIT Press, 1951.
12. F. W. Grover, “Inductance Calculations: Working Formulas and Tables”, D. Van Nostrand, 1946.
13. L. Umanand and S. R. Bhat, “Design of Magnetic Components for Switched Mode Power Converters”, New Age International Ltd. Publ., India, 1992.
14. Philips, “Ferroxcube: Soft Ferrites and Accessories”, Data Book, June 2000, www.ferroxcube.com.
15. Epcos, “Ferrites and Accessories”, Data Book, August 2001, www.epcos.com.
16. D.Y. Chen, “Comparison of high frequency magnetic core losses under two different driving conditions: A sinusoidal voltage and a square-wave voltage”, *IEEE PESC Record* , 1978.
17. F. D. Tan, J. L. Vollin and S. M. Cuk, “A practical approach for magnetic core-loss characterization”, *IEEE Trans. on Power Electronics*, vol. 10 , No. 2 , 3/1995.
18. W. Roshen, “Ferrite Core Loss for Power Magnetic Components Design”, *IEEE Trans. on Magnetics* , vol. 27, no. 6, Nov. 1991.
19. J. Li, T. Abdallah, and C. R. Sullivan, “Improved Calculation of Core Loss with Nonsinusoidal Waveforms”, *IEEE Industry Applications Society Annual Meeting*, Oct. 2001, Chicago.
20. K. Venkatachalam, C. R. Sullivan, T. Abdallah, and H. Tacca, “Accurate Prediction of Ferrite Core Loss with Nonsinusoidal Waveforms using Only Steinmetz Parameters”, *COMPEL 2002*, Jun. 2002, Puerto Rico.
21. H.E. Tacca, “Flyback vs. Forward Converter Topology Comparison Based upon Magnetic Design”, *Eletrônica de Potência* , Vol. 5, no. 1, May 2000, Brazil.
22. J.Reinert, A. Brockmeyer, and R.W. A. A. De Doncker, “Calculation of Losses in Ferro- and Ferrimagnetic Materials Based on the Modified Steinmetz Equation”, *IEEE Transactions on Industry Applications*, vol. 37, no. 4, Jul./Aug. 2001.
23. A. Brockmeyer, “Dimensionerungswerkzeug für magnetische Bauelemente in Stromritchteranwendungen”, Ph.D. dissertation, Inst. Power Electron., Aachen, Germany, 1997.
24. A. Brockmeyer, “Experimental evaluation of the influence of dc-premagnetization on the properties of power electronic ferrites”, *Applied Power Electronics Conference and Exposition 1996 (APEC’96)*, Vol. 1, 1996.

25. R. Ridley and A. Nace, "Modeling ferrite core losses", *Switching Power Magazine* , January 2002.
26. M. Amar and R. Kaczmarek, "A general formula for prediction of iron losses under nonsinusoidal voltage waveforms", *IEEE Trans. on Magnetics*, vol. 31 , No. 5 , Sept.1995.
27. V. Vorpérian, "Using fractals to model eddy-current losses in ferromagnetic materials", *Switching Power Magazine* , January 2002.
28. W. K. Mo, D. K. W. Cheng, and Y. S. Lee, "Simple Approximations of the DC Flux Influence on the Core Loss Power Electronic Ferrites and Their Use in Design of Magnetic Components", *IEEE Transactions on Industrial Electronics*, vol.44, no. 6, Dec. 1997.
29. E. Cardelli, L. Fiorucci, and E. Della Torre, "Estimation of MnZn ferrite core losses in magnetic components at high frequency", *IEEE Trans. on Magnetics*, Vol. 37, No. 4, July 2001.
30. A. Balakrishnan, W. T. Joines, and T. G. Wilson, "Air-gap reluctance and inductance calculations for magnetic circuits using a Schwarz-Christoffel transformation", *IEEE Trans. on Power Electronics* , Vol. 12, No. 4, July 1997.
31. J. Buck, "Automatic hysteresisgraph speeds accurate analysis of soft magnetic materials", *PCIM*, February 2000.
32. J. A. Ferreira and J. D. van Wyk, "Experimental evaluation of losses in magnetic components for power converters", *IEEE Trans. on Industry Applications*, Vol. 27, No. 2, March/April 1991.
33. S.-C Wang and C.-L. Chen, "PC-based apparatus for characterizing high frequency magnetic cores", *IEE Proc. - Sci. Meas. Technology* , Vol. 146, no. 6, U.K., Nov. 1999.
34. Iwatsu, "SY-8232 B-H analyzer data sheet", www.iwatsu.co.jp/tme/pdf/english/sy-8232_e.pdf .
35. R. Linkous, A. W. Kelley, and K. C. Armstrong, "An improved calorimeter for measuring the core loss of magnetic materials", *IEEE Applied Power Electronics Conf. and Expo. 2000 (IEEE - APEC 2000).*
36. V. Leonavicius, M. Duffy, C.O. Mathúna, and U. Boeke, "Comparison of different techniques to realise PFC boost inductor", *IEEE Applied Power Electronics Conference and Exposition 2002 (IEEE-APEC 2002)*, Vol. 2, 2002.
37. C. Larouci, J. P. Ferrieux, L. Gerbaud, J. Roudet, and S. Catellani, "Experimental evaluation of the core losses in the magnetic components used in PFC converters. Application to optimize the flyback structure losses", *IEEE Applied Power Electronics Conference and Exposition 2002 (IEEE-APEC 2002)*, Vol. 2, 2002.
38. J. Liu, T. G. Wilson Jr., R. C. Wong, R. Wunderlich, and F. C. Lee, "A method for inductor core loss estimation in power factor correction applications", *IEEE Applied Power Electronics Conference and Exposition 2002 (IEEE-APEC 2002)*, Vol. 2, 2002.
39. G. D'Antona et al., "AC measurements via digital processing of Rogowski coils signal", *IEEE Instrumentation and Measurement Technology Conference* , Anchorage, USA, May 2002.
40. W. F. Ray and C. R. Hewson, "High performance Rogowski current transducers", *IEEE Industry Applications Conference* , 2000.
41. W. F. Ray, "Rogowski transducers for high bandwidth high current measurement", *IEE Colloquium on Low Frequency Power Measurement and Analysis* (Digest No. 1994/203), U.K., 1994.
42. W. F. Ray, "The use of Rogowski coils for low amplitude current waveform measurement", *IEE Colloquium on Measurement Techniques for Power Electronics*, U.K., 1992.
43. C. Alarcón, A. Godel, M. Pupareli, "Proyecto de inductores con circulación de C.A. y C.C. superpuestas", *Rev. Telegráfica Electrónica*, Buenos Aires, 11/1977.